Accepted for publication in Physical Review D

hep-ph/9509360
MIT-CTP#2359
INFNCA-TH-94-9

# Contrasting Real-time Dynamics with Screening Phenomena at Finite Temperature

Suzhou Huang[(1,2)*] and Marcello Lissia[(1,3)*]

[(1)] *Center for Theoretical Physics, Laboratory for Nuclear Science and Department of Physics, Massachusetts Institute of Technology, Cambridge, Massachusetts 02139*[†]

[(2)] *Department of Physics, FM-15, University of Washington, Seattle, Washington 98195*

[(3)] *Istituto Nazionale di Fisica Nucleare, via Ada Negri 18, I-09127 Cagliari, Italy*[†]
*and Dipartimento di Fisica dell'Università di Cagliari, I-09124 Cagliari, Italy*

(August 1995; revised version January 1996)



## Abstract

We discuss the interpretation of Euclidean correlation functions at finite temperature ($T$) and their relationship with the corresponding real-time Green's functions. The soluble 2+1 dimensional Gross-Neveu model in the large-$N$ limit is used throughout as a working example. First, the real-time bound state, identified as an elementary excitation at finite $T$, is solved. The bound state mass, the dispersion relation at low momenta, the coupling constant and decay constant are calculated. To characterize the structure of the bound state the on-shell form factor is carefully introduced and calculated. Then we examine the corresponding screening state and contrast the screening mass, coupling constant, decay constant and the screening Bethe-Salpeter amplitude with the real-time quantities. We find that, although they can be used as qualitative indicators in the low-$T$ regime, the screening states at finite $T$ in general do not reflect the properties of the corresponding real-time bound states. Besides, other relevant issues, such as the subtlety of the real-time manifestation of conservation laws due to some internal symmetries at $T \neq 0$, the temperature dependence of the pseudoscalar spectral function and its sum rule, and the high-$T$ limit of the screening state and its implications to the dimensional reduction, are also discussed in detail.

11.10.Wx,11.15.Pg,11.30.-j,11.10.Kk,11.55.Hx

## I. INTRODUCTION

The formulation of QCD, or any other field theory, at finite temperature is well-established and several equivalent approaches exist. Nevertheless, since finite temperature systems are determined not only by their ground states but also by all the excited states, the study of finite temperature field theory really involves different physics with respect to the zero temperature case and different concepts need to be introduced [1].

In the existing literature the real-time dynamics is mainly discussed in a perturbative context. However, we are often interested in non-perturbative real-time physics. Typical non-perturbative methods for QCD calculation at finite $T$ are the operator product expansion and lattice simulations. Both these approaches are intrinsically Euclidean and limited to static properties. The possibility of extracting real-time information from these Euclidean quantities needs to be addressed. Due to the lack of experimental data, we do not have enough intuition to guide our approaches. Therefore, it is particularly useful to have some exact results which could provide us with insights into such matter. However, demanding exact solutions often implies a sacrifice in the direct phenomenological relevance.

In this paper, we address these issues in the U(1) chirally symmetric Gross-Neveu model [2] in $2+1$ dimensions and in the large-$N$ limit: this soluble model allows us to perform exact calculations both for real-time and screening dynamics. This model is often used in the literature [3,4] whenever exact results are required and, besides, some relevance to QCD is also desired. In fact, the Gross-Neveu model has several features in common with QCD. For instance, this model undergoes a chiral phase transition at finite $T$, as it is expected to happen in QCD, providing a good place for a qualitative modeling of the temperature dependence of real-time dynamics. However, some caution is needed: the Gross-Neveu model is not confining and, therefore, not every physical interpretation of the singularities associated to quark and antiquark can be literarily applied to QCD.

More specifically, we solve the real-time bound state and study its properties as functions of temperature. We calculate its mass, its coupling constant, its decay constant and its spectral function. In addition, we carefully characterize the size of this bound state by calculating its on-shell form factor. Similarly, we also solve the corresponding screening state by calculating the screening mass, coupling, decay constant, and the screening Bethe-Salpeter amplitude. The choice of screening observables, and of the corresponding real-time ones, has been suggested from the available lattice calculations [5,6]. Eventually, we contrast the real-time observables and the corresponding screening ones.

While some of the results presented here can be found in the existing literature, and we include them only to make the presentation of our points coherent and self-contained, others are less well-known. Among these new, or insufficiently discussed, topics we would like to emphasize the following.

(1) Due to the lack of Lorentz invariance at finite $T$ a general amplitude $A(\omega, \boldsymbol{p})$ has often very different functional dependences on $\omega^2$ and $\boldsymbol{p}^2$. An obvious consequence of this non-uniformness is, for example, the non-covariant energy-momentum dispersion relation for elementary excitations. A less obvious but more interesting consequence is related to how conservation laws due to some internal symmetries manifest themselves in various physical processes. The Goldberger-Treiman relation and the effective charge of the pion are used as illustrations.

(2) To characterize the structure of a bound state at finite $T$ in a physical way we introduce the on-shell form factor in the elastic limit. The peculiarity of the relevant kinematic condition and the existence of an additional form factor are carefully addressed. Then we isolate the singularity structure that characterizes the on-shell form factor as a function of the spatial momentum transfer and, therefore, determine the size of the bound state.
(3) We derive an exact sum rule, which states that the zeroth moment of the pseudoscalar spectral function is temperature independent.
(4) The screening Bethe-Salpeter amplitudes in scalar and pseudoscalar channels are calculated explicitly.
(5) We obtain the asymptotic formula for the screening mass in the high-$T$ limit and show that this result demonstrates the failure of dimensional reduction in this model. The reason of this failure is also explained.

Strictly speaking, the 2+1 dimensional Gross-Neveu model with a continuous symmetry has no finite-$T$ phase transition beyond the leading order in $1/N$, due to the severe infrared singularity associated with massless Goldstone bosons. One might question the relevance of our results at leading order in $1/N$. This problem can be avoided by working in $2+\epsilon$ spatial dimensions ($0 < \epsilon < 1$), where the infrared catastrophe is absent. Since the limit $\epsilon \to 0$ is smooth at the leading order in $1/N$, our results presented in this paper should be understood as such. We could have also addressed the same questions in the 3+1 dimensional Nambu-Jona-Lasinio model [7]. However, since our present interest is more related to answering conceptual questions rather than finding direct phenomenological applications, we prefer to use the 2+1 Gross-Neveu model because of its renormalizability. Moreover, we believe that the qualitative physics associated with the chiral restoration at finite $T$ is similar in all these models, independently of their dimensionality. In any case, we shall take notice of those results that are directly linked to the specific dimensionality.

The paper is organized as follows. First, we give, in Sec. II, a brief pedagogical review of how real-time dynamics is formulated at finite $T$. Then, in Sec. III, we introduce the model and collect all those results that are useful in the rest of the paper. The real-time pseudoscalar bound state and its properties are calculated in Sec. IV. In this same section we also discuss the Goldberger-Treiman relation, the on-shell form factor and derive a sum rule for the spectral function. The screening state is discussed in Sec. V, where we also contrast minutely the real-time bound state and the screening state. The last subsection of Sec. V is dedicated to the high temperature limit of the screening state and to the implications that this result has for dimensional reduction. We reserve Sec. VI to a summary of our work and to conclusions.

## II. GENERAL INTERPRETATION

In this section we review the connection between correlation functions, which are the typical output of theoretical calculations, and the real-time response of a system to external perturbations. The following material is most likely well-known to experts [8]; nonetheless, since we are specifically concerned with the proper interpretation of Euclidean correlation functions, we find useful to include it here as a convenient reminder.

An experimentalist perturbs a system with an external probe, and then measures the

effect of this perturbation with some detector. In a given theory we describe this external perturbation using an interaction Hamiltonian of the form

$$\hat{H}_{\rm ext}(t) = \int d\boldsymbol{x} J(\hat{\psi}(t,\boldsymbol{x}))V_{\rm ext}(t,\boldsymbol{x})\,, \qquad \text{with} \quad V_{\rm ext}(t<0,\boldsymbol{x}) = 0\,, \tag{1}$$

where $V_{\rm ext}(t,\boldsymbol{x})$ is the external perturbation, which is switched on at $t = 0$, and couples to the system through the current $J(\hat{\psi}(t,\boldsymbol{x}))$ (the hat indicates operators). The system is described by a state, or ensemble of states of the Hamiltonian, and the measurement of the response to the perturbation is performed through another current, which can be the same as the one that couples to the perturbation. For example, we may perturb the system with an external electric field, which couples to the charge density, and measure the resulting change in the same charge density. Therefore, we typically measure the change of the expectation value of a given current due to the presence of the perturbation:

$$\delta\langle J(\hat{\psi}(t))\rangle \equiv \langle J(\hat{\psi}(t))\rangle_{\rm ext} - \langle J(\hat{\psi}(t))\rangle_0\,, \tag{2}$$

where $\langle\hat{A}\rangle_{\rm ext}$ is the expectation value of the operator $A$ in the state (or ensemble of states) describing the system in the presence of the external perturbation, and $\langle A\rangle_0$ the corresponding expectation value in the unperturbed system. Here and in the following we drop the spatial label for simplicity.

If the perturbation is weak, we can expand in the perturbation, and keep only the term linear in the external field. Then the linear response of the system to the perturbation is simply proportional to the retarded correlation function:

$$\delta\langle J(\hat{\psi}(t))\rangle = \int_{-\infty}^{\infty} dt' G^R(t-t')V_{\rm ext}(t'), \tag{3a}$$

where the retarded correlation is defined as

$$G^R(t) = \theta(t)\frac{{\rm Tr}\left(e^{-\hat{H}_0/T}[J(\hat{\psi}(t))\,,\,J(\hat{\psi}(0))]\right)}{{\rm Tr}\left(e^{-\hat{H}_0/T}\right)} \tag{3b}$$

and $\hat{\psi}(t) = e^{it\hat{H}_0}\hat{\psi}(0)e^{-it\hat{H}_0}$, $\hat{H}_0$ is the unperturbed Hamiltonian, and we consider a system in thermal equilibrium at temperature $T$. The physical content of this equation is known as the fluctuation-dissipation theorem, i.e. correlation functions of a system describe not only the correlations (fluctuations) of the system in a given channel, but also its linear response (dissipation) to weak external perturbations.

We say that the system has a (real-time) elementary excitation in the channel described by a given current, if we get a resonant (very large) response to the corresponding external perturbation at a given frequency. If we rewrite Eq. (3a) in frequency-momentum space (restoring the spatial dependence)

$$\delta\langle J\rangle(\omega,\boldsymbol{k}) = \tilde{G}^R(\omega,\boldsymbol{k})\tilde{V}_{\rm ext}(\omega,\boldsymbol{k})\,, \tag{4}$$

we can see that the appearance of a pole in the correlator as a function of $\omega$ gives this kind of resonant response, which will be called the bound state. It is clear from Eq. (4) that the

resonance frequency depends on spatial momentum $\boldsymbol{k}$: $\omega = \omega(\boldsymbol{k})$. The function $\omega(\boldsymbol{k})$ is the so-called dispersion relation for the excitation.

Alternatively, we can use a time-independent external perturbation ($\omega = 0$), and study the static response of the system. In this case, we are interested in the modification of the system in spatial distribution, e.g. how the effect of the perturbation dies out with distance (screening). In momentum space there can still exist purely imaginary poles in the retarded correlator, but now they are interpreted as pure exponential terms in the decaying response. At zero temperature only, due to Euclidean invariance for relativistic theories, there is a one to one correspondence between these poles in the imaginary momentum and the ones in frequency.

The resonant frequencies of the system (poles of the propagator) are important characteristics of the system, but they are not the only information we get from experiment (and from the propagator). The strength with which the external probe couples to the system is also important. For instance, excitations of the system that do not couple to the external probe may not be relevant. In the propagator, the information about the coupling strength is carried by the residue of the pole at the resonant frequency.

A nice example of the concepts we have just reviewed is the classic electron plasma probed through the charge density: $J(t, \boldsymbol{x}) = \psi^\dagger(t, \boldsymbol{x})\psi(t, \boldsymbol{x})$. The response of the plasma to a static point charge is just the well-known Debye screening

$$\delta\langle J(\boldsymbol{x})\rangle \propto \int dt\, G^R(t, \boldsymbol{x}) \propto e^{-m_D|\boldsymbol{x}|}\,, \tag{5}$$

and the corresponding pole in the static propagator,

$$\tilde{G}^R(\omega = 0, \boldsymbol{k}) \propto \frac{1}{\boldsymbol{k}^2 + m_D^2}\,, \tag{6}$$

is the Debye mass: $m_D^2 = 8\pi n_0 e^2/kT$ ($n_0$ and $e$ are the electron density and charge, respectively).

But the plasma also possess real-time excitations, plasmons, with characteristic frequency $\omega_{\rm ph}^2(\boldsymbol{k} = 0) = 4\pi e^2 n_0/m_e$, where $m_e$ is the electron mass. These excitations are described, near the plasmon pole, by the Green's function

$$\tilde{G}^R(\omega, \boldsymbol{k}) \propto \frac{1}{\omega - \omega_{\rm ph}(\boldsymbol{k}) + i\gamma}\,, \tag{7}$$

where $\gamma$ is the damping rate which gives a finite width to the plasmon. The frequency-momentum (or dispersion) relation for plasmons is $\omega_{\rm ph}^2(\boldsymbol{k}) = \omega_{\rm ph}^2(0) + \boldsymbol{k}^2$.

From the preceding example it is quite clear that in general real-time excitations and screening states describe different physics. Nevertheless, there is a connection between measurements in Minkowski and Euclidean space. In general, causality and unitarity make possible the following dispersion relation for the correlation function

$$\tilde{G}^R(\omega, \boldsymbol{k}) = \frac{1}{\pi}\int_{-\infty}^{\infty} du\, \frac{\rho(u, \boldsymbol{k})}{u - \omega - i\epsilon}\,, \tag{8}$$

where the spectral function $\rho$ is proportional to the total cross-section in the given channel. It is important to realize that the dispersion relation at finite $T$ is in frequency only and the

spatial momentum is treated as a parameter. In the plasmon example, if the plasmon were the only excitation of the system, the spectral density $\rho$ would just be the on-shell condition for the plasmon:

$$\rho(u, \boldsymbol{k}) = \lambda^2 \, \epsilon(u) \, \delta(u^2 - \omega_{\rm ph}^2(\boldsymbol{k})) \, . \tag{9}$$

The power of the dispersion relation is that the physical content of the correlation is entirely embodied in the spectral function $\rho$, which determines the correlation in the whole complex plane, apart from a possible additive polynomial in $\omega$. For instance, if we analytically continue the correlation function to imaginary frequencies, we obtain

$$\tilde{g}^R(\omega, \boldsymbol{k}) = \frac{1}{\pi} \int_{-\infty}^{\infty} du \frac{\rho(u, \boldsymbol{k})}{u - i\omega} \, . \tag{10}$$

This analytically continued correlation function calculated at the Matsubara frequencies $\omega_n = (2n-1)\pi T$ (for fermions) is the discrete Fourier transform of the correlator calculated in the Euclidean region (finite temperature correlator):

$$g(\tau) = \frac{\mathrm{Tr}\left(e^{-\hat{H}_0/T} J(\hat{\psi}(\tau)) J(\hat{\psi}(0))]\right)}{\mathrm{Tr}\left(e^{-\hat{H}_0/T}\right)} \tag{11}$$

where $\hat{\psi}(\tau) = e^{\tau \hat{H}_0} \hat{\psi}(0) e^{-\tau \hat{H}_0}$. This formula is valid in the interval $0 < \tau < 1/T$, while for $\tau$ outside this interval we can use the periodicity condition, which for fermions reads $g(\tau + 1/T) = -g(\tau)$ (it follows from the periodicity of the trace and the anticommutation property of the fermionic fields).

Vice versa, if we know the correlation function at the discrete set of Euclidean points specified by the Matsubara frequencies, the analytic continuation $\omega_n \to -i\omega \pm \epsilon$ provides us with the retarded/advanced correlation for continuous real-time frequency. This continuation is unique only when the expression of the correlation function is explicitly free of singularity in the entire $\omega$-plane except on the real axis and obeys certain convergence property at $|\omega| \to \infty$ [8].

Finally, due to the lack of Lorentz invariance at finite $T$, a general Green's function $G(\omega, \boldsymbol{p})$ often has very different functional dependence on $\omega^2$ and on $\boldsymbol{p}^2$. For example, $G(0, \boldsymbol{0})$ strongly depends on the order in which we take the limits $\omega \to 0$ and $\boldsymbol{p} \to 0$, i.e. $G(0^+, \boldsymbol{0}) \equiv \lim_{\omega \to 0} \lim_{\boldsymbol{p} \to 0} G(\omega, \boldsymbol{p})$ is usually different from $G(0, \boldsymbol{0}^+) \equiv \lim_{\boldsymbol{p} \to 0} \lim_{\omega \to 0} G_(\omega, \boldsymbol{p})$. (The innocent looking function $(x+y)/(x-y)$ in the limit of $x$, $y \to 0$ illustrates the relevant subtlety.) Of course, the physics of the specific process selects which of the two order is relevant. In particular, $G(0^+, \boldsymbol{0})$ is intrinsically Minkowskian, because it represents a process whose characteristic time is much shorter than the heat-bath response-time. We shall then call this kind of processes fast processes. Correspondingly, $G(0, \boldsymbol{0}^+)$ is intrinsically Euclidean and the related processes are called slow processes, since the thermal environment has enough time to respond to the external perturbation. As we will see later, conservation laws due to internal symmetries only hold in fast processes. In slow processes the apparent violation of conservation laws should be understood in the sense of the grand canonical ensemble, not as the violation of the fundamental physics laws.

## III. THE GROSS-NEVEU MODEL

In this section we introduce the Gross-Neveu model [2] in $2+1$ dimensions, and present its main features at finite temperature. Corresponding formulae for the model in $1+1$ dimensions can be found in Ref. [9].

### A. Lagrangian

The Gross-Neveu model is defined by the Lagrangian density

$$\mathcal{L} = \bar{\psi} i\gamma \cdot \partial\psi + \frac{g^2}{2N}\left[(\bar{\psi}\psi)^2 + (\bar{\psi} i\gamma_5 \psi)^2\right], \tag{12a}$$

where $\psi$ is a 4-component Dirac spinor with the color indices implicit. Equivalently, we can write

$$\mathcal{L} = \bar{\psi} i\gamma \cdot \partial\psi - \bar{\psi}(\sigma + i\pi\gamma_5)\psi - \frac{N}{2g^2}(\sigma^2 + \pi^2), \tag{12b}$$

where $\sigma$ and $\pi$ are the auxiliary scalar and pseudoscalar bosonic fields, respectively. We study this model in the limit $N \to \infty$ with the coupling constant $g^2$ fixed. This Lagrangian is invariant under a continuous $U(1)$ chiral symmetry that is dynamically broken at low $T$.

### B. Effective potential and mass generation

The standard approach of the effective potential at finite temperature [10] yields the critical temperature and the dynamically generated mass. To the leading order in $1/N$, the effective potential for $\sigma$ and $\pi$ fields is given by the one-loop expression

$$V_{\text{eff}}(\sigma,\pi) = \frac{N}{2g^2}(\sigma^2+\pi^2) - 2N\int \frac{d^2k}{(2\pi)^2}\, T \sum_{n=-\infty}^{+\infty} \ln\left[k^2 + \omega_n^2 + \sigma^2 + \pi^2\right], \tag{13}$$

where $\omega_n = (2n-1)\pi T$. Up to an irrelevant constant the sum over $n$ can be done yielding

$$V_{\text{eff}}(\sigma,0) = \frac{N}{2g^2}\sigma^2 - 2N\int \frac{d^2k}{(2\pi)^2}\left\{\sqrt{k^2+\sigma^2} + 2T\ln\left[1+\exp(-\sqrt{k^2+\sigma^2}/T)\right]\right\}. \tag{14}$$

In this last and the following equations we have used the symmetry of the Lagrangian, and rotated the $(\sigma,\pi)$ field in the $\sigma$ direction making $\pi = 0$. Alternatively, we can read $\sigma$ in the following formulae as representing $\sqrt{\sigma^2+\pi^2}$. The integral is divergent, and a high momentum cutoff $\Lambda$ is required. We make $V_{\text{eff}}$ finite by adding a counterterm of the form

$$\mathcal{L}_{\text{CT}} = -\frac{N}{2}(\sigma^2+\pi^2)\left(\frac{\Lambda}{\pi} - \frac{\kappa}{\pi}\right), \tag{15}$$

i.e. we have defined the bare coupling constant $\pi/g_B^2 = \pi/g^2 - \kappa + \Lambda$, with $g^2 \equiv g^2(\kappa)$ the renormalized coupling constant.

Then, the renormalized effective potential is

$$V_{\rm eff}(\sigma,0)=\frac{N}{\pi}\left\{\frac{1}{3}|\sigma|^3-\frac{\mu}{2}\sigma^2+T^3\int_0^{\sigma^2/T^2}dz\,\ln\left[1+\exp(-\sqrt{z})\right]\right\}, \tag{16}$$

where $\mu\equiv\kappa-\pi/g^2(\kappa)$, which is independent of the renormalization scale $\kappa$, will turn out to be the dynamical quark mass at $T=0$.

The quantum theory is determined by the fluctuations around the minimum of the effective potential, which we find from the stationary condition

$$\left.\frac{\partial V_{\rm eff}(\sigma,0)}{\partial\sigma}\right|_{\sigma=\sigma_m}=\frac{N}{\pi}\sigma_m\left\{\sigma_m-\mu+2T\,\ln\left[1+\exp(-\sigma_m/T)\right]\right\}=0\,. \tag{17}$$

When $T>T_c$ (high $T$ phase), the expression in braces is positive definite, and the only solution to Eq. (17) is $\sigma_m=0$ (symmetric phase). The critical $T_c$ is the value of $T$ for which the expression in braces is zero with $\sigma_m=0$, i.e. $T_c=\mu/\ln 4$.

When $T<T_c$, the expression in braces is zero for the following value of $\sigma_m$:

$$\sigma_m(T)=\mu\left(1-\frac{T}{T_c}\right)+2T\,\ln\left[1+\sqrt{1-4\exp(-\mu/T)}\right], \tag{18}$$

which is the absolute minimum of the effective potential, Eq. (16), while the other stationary point, $\sigma=0$, is a maximum for these values of $T$. Consequently, the symmetry is dynamically broken and the corresponding quark mass is $m(T)=\sigma_m(T)$.

In Fig. 1 we plot the dynamically generated mass as a function of temperature, i.e. Eq. (18): it goes exponentially to $\mu$ in the zero temperature limit, while it approaches zero as $2\sqrt{\mu(T_c-T)}$ for $T$ approaching $T_c$ from below.

For later convenience we define the following function of $T$, which is proportional to the first derivative of $V_{\rm eff}(\sigma,\pi)$ with respect to $\sigma^2$ evaluated at $(\sigma=m,\pi=0)$,

$$R(T)\equiv\mu-m(T)-2T\,\ln[1+\exp(-m(T)/T)]=\begin{cases}0 & \text{if } T\le T_c\\ \mu\left(1-\frac{T}{T_c}\right) & \text{if } T>T_c\end{cases}. \tag{19}$$

### C. Pseudoscalar Bubble Graph

In this model, the only one-particle irreducible loop graph (in the large $N$ limit) that is relevant for our purpose is the pseudoscalar bubble graph $\Pi_P$. In order to extract the bound state and screening states, we need this graph in Minkowski space for general $(\omega,\boldsymbol{p})$. We first use the imaginary-time formalism to perform the loop integral:

$$i\Pi_P(\omega,\boldsymbol{p})=NT\sum_{n=-\infty}^{+\infty}\int^{\Lambda}\frac{d^2\boldsymbol{k}}{(2\pi)^2}{\rm Tr}\left\{i\gamma_5\frac{i}{k\cdot\gamma-m}i\gamma_5\frac{i}{k\cdot\gamma-p\cdot\gamma-m}\right\}, \tag{20}$$

where $k=(i\omega_n,\boldsymbol{k})$, $p=(i\omega,\boldsymbol{p})$, $\omega_n=(2n-1)\pi$ with $n=0,\pm1,\pm2,\cdots$, and $\omega=2\pi l$ with $l=0,\pm1,\pm2,\cdots$. The sum over frequencies can be performed by using standard contour integral techniques [10], and we obtain:

$$i\Pi_P(\omega,\boldsymbol{p}) = -N\int^{\Lambda}\frac{d^2\boldsymbol{k}}{(2\pi)^2}\frac{\tanh(E_k/2T)}{2E_k}\left\{\frac{4k\cdot p}{p^2-2k\cdot p}-\frac{4k\cdot p}{p^2+2k\cdot p}\right\}_{k_0=E_k}, \tag{21}$$

where $E_k^2 = m^2+\boldsymbol{k}^2$. The above equation is infinite and can be made finite by adding the contribution from the counterterm $i\Pi_{\rm CT} = \partial^2\mathcal{L}_{\rm CT}/\partial\sigma^2 = -N(\Lambda-\pi/g^2-\mu)/\pi$. We then analytically continue $\omega$ into the entire complex plane.

For calculating the bound state mass, it is sufficient to have the expression for zero external momentum in the region $0<\omega^2<4m^2$ for the pseudoscalar channel:

$$\begin{aligned} i\Pi_P(\omega) &= \frac{N}{g^2}+\frac{N}{\pi}R(T)+\frac{N\omega^2}{4\pi}\int_m^\infty dE\,\tanh\frac{E}{2T}\,\frac{1}{E^2-\omega^2/4} \\ &= \frac{N}{g^2}+\frac{N}{\pi}\left\{R(T)+\frac{\omega}{4}\,\ln\left[\frac{2m+\omega}{2m-\omega}\right]-\frac{\omega^2}{4}\int_m^\infty dE\,\frac{2}{1+e^{E/T}}\,\frac{1}{E^2-\omega^2/4}\right\}. \end{aligned} \tag{22}$$

In the region $\omega^2>4m^2$, which is needed for the spectral function, the bubble develops an imaginary part, and the corresponding formulae are:

$$\mathrm{Re}\,[i\Pi_P(\omega)] = \frac{N}{g^2}+\frac{N}{\pi}\left\{R(T)+\frac{\omega}{4}\,\ln\left[\frac{\omega+2m}{\omega-2m}\right]-\frac{\omega^2}{4}\fint_m^\infty dE\,\frac{2}{1+e^{E/T}}\,\frac{1}{E^2-\omega^2/4}\right\} \tag{23a}$$

$$\mathrm{Im}\,[i\Pi_P(\omega)] = \frac{N}{4}\omega\tanh\frac{\omega}{4T}, \tag{23b}$$

where $\fint$ indicates the principal part of the integral.

For studying the screening phenomena we need the pseudoscalar bubble, Eq. (20), in the Euclidean region for $\omega=0$, i.e. in the static limit. It is convenient to expand the hyperbolic tangent by using the formula

$$\tanh x = \sum_{n=-\infty}^{+\infty}\frac{x}{x^2+[\pi(n-1/2)]^2} \tag{24}$$

and perform the $\boldsymbol{k}$-integral. The resulting expression is

$$\frac{\pi}{N}i\Pi_P(i\omega\to 0,\boldsymbol{p}) = \frac{\pi}{g^2}+R(T)-T\sum_{n=-\infty}^{\infty}\sqrt{\frac{\boldsymbol{p}^2}{4M_n^2+\boldsymbol{p}^2}}\,\ln\left[\frac{\sqrt{4M_n^2+\boldsymbol{p}^2}+\sqrt{\boldsymbol{p}^2}}{\sqrt{4M_n^2+\boldsymbol{p}^2}-\sqrt{\boldsymbol{p}^2}}\right], \tag{25}$$

where $M_n^2\equiv\omega_n^2+m^2(T)$.

### D. Two-point function

To the leading order in $1/N$ the retarded two-point function for pseudoscalar current involves only a sum over a geometric series of the pseudoscalar bubble graph:

$$\langle J_5J_5\rangle_T^R(\omega,\boldsymbol{p}) \equiv \int d\boldsymbol{x}dt\,\exp(i\omega t-i\boldsymbol{p}\cdot\boldsymbol{x})\theta(t)\langle[J_5(t,\boldsymbol{x}),\bar{J}_5(0,\boldsymbol{0})]\rangle_T = \frac{i\Pi_P(\omega,\boldsymbol{p})}{1-(ig^2/N)\Pi_P(\omega,\boldsymbol{p})}, \tag{26}$$

where $J_5(t,\boldsymbol{x}) = \bar{\psi}(t,\boldsymbol{x})\, i\gamma_5\, \psi(t,\boldsymbol{x})$, and we have renormalized the two-point function in such a way that its lowest order coincides with the renormalized bubble.

When the above equation has a pole in real frequency $\omega$ at a given spatial momentum $\boldsymbol{p}$, this pole is identified as the elementary excitation or the bound state. In the static limit ($\omega = 0$), on the other hand, the lowest singularity for $-\boldsymbol{p}^2$, denoted by $\tilde{m}^2$, corresponds to the screening mass.

## IV. REAL-TIME DYNAMICS

In this section the real-time dynamics is studied. We first solve the bound state in the pseudoscalar channel, including the bound state mass, with its dispersion relation for small momenta, the coupling and decay constants. The Goldberger-Treiman relation is examined carefully. We then calculate the on-shell form factor and the charge radius. Finally, the spectral function and its sum rule are derived.

### A. Pseudoscalar Bound State

As discussed in section II, a physical excitation in a given channel is signaled by a pole in the corresponding correlation function. Therefore, a bound state in the pseudoscalar channel (there is no elementary pseudoscalar excitation in the Lagrangian) exists, if there is a solution to the equation obtained by equating to zero the denominator of Eq. (26)

$$\begin{aligned} 0 &= 1 - \frac{g^2}{N} i\Pi_P(\omega = m_\pi) \\ &= R(T) + \frac{m_\pi}{4} \ln\left[\frac{2m + m_\pi}{2m - m_\pi}\right] - \frac{m_\pi^2}{4} \int_m^\infty dE\, \frac{2}{1 + e^{E/T}}\, \frac{1}{E^2 - m_\pi^2/4}\,, \end{aligned} \tag{27}$$

where we have used the expression for the pseudoscalar bubble, Eq. (22), valid for $0 < \omega^2 < 4m^2$. This equation has always the solution $m_\pi = 0$, which is lower than the energy of the unbound particles $2m$, as long as $T < T_c$ ($R(T) = 0$). The study of the residue associated with this solution can also help in determining the fate of the bound state when $T \to T_c$.

As long as we are only interested in the bound state mass, the bubble calculated at zero momentum $\boldsymbol{p}$ is sufficient. However, it is also instructive to calculate the energy as a function of momentum. In fact the system at finite temperature has a preferred reference frame, the heat bath, and we expect an explicit loss of covariance for the energy-momentum dispersion relation. To this end, we perform the calculation of the bound state energy retaining terms up to the first order in $\boldsymbol{p}^2$ and $\omega^2$ ($\omega^2$ is also small in the limit of small $\boldsymbol{p}^2$). The bubble in this limit can be written as:

$$i\Pi(\omega, \boldsymbol{p}) = \frac{N}{g^2} + \frac{N}{4\pi m} \left\{ \omega^2 \int_1^\infty \frac{dx}{x^2} \tanh\frac{mx}{2T} - \frac{\boldsymbol{p}^2}{2} \int_1^\infty dx \left(\frac{1}{x^2} + \frac{3}{x^4}\right) \tanh\frac{mx}{2T} \right\}, \tag{28}$$

where we have dropped terms of order $\boldsymbol{p}^4$, $\omega^4$, $\boldsymbol{p}^2\omega^2$ and higher. It should be emphasized that when obtaining Eq. (28) the bubble is expanded in powers of $\boldsymbol{p}^2$ first, and then the

corresponding coefficients are expanded in powers of $\omega^2$. Again by solving the bound state equation $i\Pi = N/g^2$, we find

$$\omega^2(\boldsymbol{p}^2) = v^2(T)\,\boldsymbol{p}^2 + O(\boldsymbol{p}^4) \tag{29a}$$

where the function

$$v^2(T) = \frac{\int_1^\infty dx\,(x^{-2} + 3x^{-4})\tanh(mx/2T)}{2\int_1^\infty dx\,x^{-2}\tanh(mx/2T)}\,, \tag{29b}$$

has the following limits: $\lim_{T\to 0} v^2(T) = 1$ , as it should, and $\lim_{T\to T_c} v^2(T) = 1/2$. The fact that $v^2(T) < 1$ implies that the speed of the pion is reduced by the thermal environment, even though the pion is still massless.

As stated in section II, the bound state coupling constant to a quark-antiquark pair is given by the residue of the full pion propagator on the mass-shell

$$g_\pi^2(T) = \left(\frac{\partial}{\partial\omega^2} i\Pi_P(\omega)\right)^{-1}_{\omega=m_\pi} = \frac{4\pi m}{N}\left(\int_1^\infty \frac{dx}{x^2}\,\tanh\frac{mx}{2T}\right)^{-1}\,, \tag{30}$$

which is also proportional to the residue of the pole of the correlation function, Eq. (26), at $\omega = m_\pi$.

The dependence of $g_\pi^2(T)$ on temperature is shown in Fig. 2. When $T \to 0$, $m \to \mu$, and $g_\pi^2 \to 4\pi\mu/N$ (zero temperature limit). When $T \to T_c^-$, $m(T) \to 0$, and $g_\pi^2(T) \to 0^+$. In this last case, the coupling $g_\pi^2(T)$ approaches zero logarithmically: $\lim_{T\to T_c^-} g_\pi^2(T) \propto (\log m)^{-1} \propto [\log(T_c - T)]^{-1}$. In contrast, the corresponding coupling in the four dimensional Nambu-Jona-Lasinio model in the chiral limit approaches a finite constant at $T_c - 0^+$, and then it jumps to zero for $T > T_c$ [7].

The bound state solution in the pseudoscalar channel for $T = T_c$ has the same energy of two free quarks, and one might wonder about the fate of the bound state in the limit $T \to T_c^-$. The coupling constant result gives us a clear answer suggesting that the bound state disappears at the phase transition. More precisely, we should conclude that the pseudoscalar meson decouples from its constituents at the phase transition.

### B. The Goldberger-Treiman relation

We can also introduce a pion decay constant defined as the residue of the axial current correlation function at the pion pole (this definition at $T = 0$ yields the usual expression $\langle 0|J_\mu^5|\pi(p)\rangle = -ip_\mu f_\pi$). So we need to calculate the axial-pseudoscalar bubble graph $A_\mu(i\omega, \boldsymbol{p})$, defined by replacing in Eq.(20) one of the $i\gamma_5$ with $\gamma_\mu\gamma_5$. It is easy to verify that $A_\mu(i\omega, \boldsymbol{p}) = p_\mu A(i\omega, \boldsymbol{p})$ with

$$A(i\omega, \boldsymbol{p}) = \frac{NT}{\pi}\sum_n \int_0^1 d\alpha\,\frac{m}{\omega_n^2 + m^2 + \alpha\omega(\omega - 2\omega_n) + \alpha(1-\alpha)\boldsymbol{p}^2}\,, \tag{31}$$

where $\omega = 2\pi l$ is the bosonic Matsubara frequency. The above equation can not be naively used to analytically continue $i\omega$ into the entire complex plane, since $i\omega$ has singularities off

the real axis. However, for calculating the pion decay constant we only need $A$ at $\boldsymbol{p} = 0$. Then the $\alpha$-integral can be done, while the sum over $n$ can be carried out by the standard contour integral technique, yielding,

$$A(i\omega, \boldsymbol{p} = 0) = \frac{N}{2\pi} \int_m^\infty dx \, \tanh\left(\frac{x}{2T}\right) \, \frac{m}{x^2 - (i\omega)^2/4} \,, \tag{32}$$

which now can be trivially continued and then put on mass-shell. Hence, the pion decay constant is given by

$$f_\pi(T) = g_\pi(T) \, A(0^+, \mathbf{0}) = g_\pi(T) \, \frac{N}{2\pi} \int_1^\infty \frac{dx}{x^2} \tanh\left(\frac{mx}{2T}\right) \,, \tag{33}$$

which is valid in the broken phase. Since there is no pion state in the symmetric phase, $f_\pi(T)$ is not defined when $T > T_c$. The vanishing of $f_\pi$ at $T = T_c$ merely reflects the fact that the chiral symmetry is restored. Using the explicit expression of $g_\pi^2(T)$, the above equation can be rewritten as

$$g_\pi(T) \, f_\pi(T) = 2m(T) \,, \tag{34}$$

which is the Goldberger-Treiman relation at finite $T$. Notice that $g_A = 1$ identically in the large-$N$ limit.

If we were not careful in using $A(0^+, \mathbf{0})$ to define $f_\pi(T)$ we would have got an expression of $f_\pi(T)$ not satisfying the Goldberger-Treiman relation. For example, if we put the axial-pseudoscalar bubble graph on the mass-shell before taking the limit $\boldsymbol{p} \to 0$, we would have effectively used $A(0, \mathbf{0}^+) = \frac{N}{2\pi} \tanh(m/2T)$ in Eq. (33). The physical reason that the pion decay should be regarded as a fast process is that the decay happens instantaneously and the thermal environment does not have enough time to respond.

At this point it is appropriate to comment on the fact that it is not trivial how, at finite temperature, the conservation laws that are the consequence of symmetries of a theory manifest themselves in the real-time dynamics. Ward identities associated with global symmetries can be straightforwardly generalized from the $T = 0$ case to finite $T$ in the Euclidean formalism. However, it is very subtle how to subsequently analytically continue these relations between Euclidean Green's functions to corresponding relations between real-time quantities and at which stage one should put the external lines on their mass-shells. Therefore, one can not simply assume that Euclidean Ward identities immediately apply also to the on-shell quantities, as was done in Ref. [11]. It appears that the validity of the conservation laws depends on the specific mathematical prescriptions, but this dependence is not arbitrary: it reflects the nature of the formulation of field theories at finite $T$ in terms of ensemble averages. Only in fast processes, where the heat bath does not have time to respond, conservation laws hold explicitly. Whereas in slow processes, where a measurement always involves the feedback of the heat bath, conservation laws are no longer manifest. We will encounter an example of such a "violation" in the next subsection.

### C. On-shell Form Factor

At any temperature the on-shell form factor in the elastic limit provides a physical measure of the size of an elementary excitation. In fact, even at finite $T$, we can imagine

the following experiment. In the heat-bath frame, we scatter a lepton off the pion. Just as in the usual zero temperature scattering, we select those leptons that have scattered off an on-shell pion rather than off something else by using the appropriate kinematic conditions. In our case, this is possible because the pion is massless, while an unbound quark-antiquark is massive. The elasticity here is important, since the kinematics selects out slow processes in which the scattered lepton sees not only the pion but also the thermal cloud around it. The size defined this way provides a snap shot of the elementary excitation immersed in an equilibrated thermal environment.

The on-shell form factor has also been studied in Ref. [12]. However, the author apparently did not realize several complications that arise when defining on-shell form factors at finite $T$, such as the proper on-shell condition at finite $T$ and the appearance of additional form factors.

On general ground, a typical three-point function with two pion lines and one photon line, as shown in Fig. 4, has the following structure in the heat-bath frame

$$f_\mu(p,p') = (p_\mu + p'_\mu)F[p^2, p'^2, p\cdot p'] + \delta_{\mu 0} G[p^2, p'^2, p\cdot p']\,. \tag{35}$$

The additional form factor $G[p^2, p'^2, p\cdot p']$ vanishes identically at $T=0$ and it is related to the heat bath. To minimize the environmental effect and hence to emphasize the intrinsic structure of the pion it is natural to use the the invariant function $F$ to define its size; to this end, we can select the spatial components $f_i(p,p')$, which receive contribution only from $F$, i.e. we consider a "magnetic scattering process".

For low energy elastic scattering, the momentum transfer is $q \equiv p' - p = (0, \boldsymbol{p}' - \boldsymbol{p})$, i.e. $p_0 = p'_0$ and $\boldsymbol{p}^2 = \boldsymbol{p}'^2$. Due to the breaking of the explicit Lorentz invariance at finite temperature, the on-shell condition for the pion does not imply $p^2 = \omega^2(\boldsymbol{p}) - \boldsymbol{p}^2 = m_\pi^2$. Therefore, there exist two independent variables in the on-shell form factors $F$ and $G$, even in the elastic limit. We choose these two independent variables to be $\omega(\boldsymbol{p})$ and $\boldsymbol{q}^2 = (\boldsymbol{p}'-\boldsymbol{p})^2$. Then the radius of the pion at finite temperature is defined as

$$\langle r^2\rangle_T \equiv -4 \lim_{\omega(\boldsymbol{p})\to m_\pi} \left\{ \lim_{\boldsymbol{q}^2\to 0} \frac{\partial \ln F[\boldsymbol{q}^2, \omega(\boldsymbol{p})]}{\partial \boldsymbol{q}^2} \right\}. \tag{36}$$

The factor of 4, rather than the usual 6, is due to the fact that we are in two spatial dimensions. This definition coincides with the usual definition at zero temperature. The overall normalization of $F[\boldsymbol{q}^2, \omega(\boldsymbol{p})]$, which depends on $T$ because the charge of the pion gets screened ($F[\boldsymbol{q}^2 = 0, \omega(\boldsymbol{p})] \le 1$ in general), does not affect the charge distribution. The limit of $\omega(\boldsymbol{p}) \to m_\pi$ is to ensure that the radius is measured in the heat-bath frame. This condition need not be imposed at zero temperature, due to the Lorentz covariance. In case one has trouble to imagine a charge radius for a massless particle, we could have included a small quark mass in the Lagrangian such that $m_\pi > 0$. This formal process is not really necessary since the limit $m_\pi \to 0$ is smooth.

The graph that gives the leading $1/N$ contribution to $F[\boldsymbol{q}^2, \omega(\boldsymbol{p})]$ is shown in Fig. 4. The advantage of probing the pion by a photon instead of a scalar, the $\sigma$, is that meson-pole dominance is avoided, consistent with our intention to emphasize the intrinsic structure. Using the pion-quark-antiquark coupling derived in the last section, we have

$$f_i(p,p') = g_\pi^2(T)\, T \sum_{n=-\infty}^{\infty} \int \frac{d^2\boldsymbol{k}}{(2\pi)^2} \frac{\mathrm{Tr}\gamma_5(k\cdot\gamma+m)\gamma_5(k\cdot\gamma-p\cdot\gamma+m)\gamma_i(k\cdot\gamma-p'\cdot\gamma+m)}{[k^2-m^2][(k-p)^2-m^2][(k-p')^2-m^2]}\,, \tag{37}$$

where $m = m(T)$ is the mass gap. In the elastic limit the momenta are $k = (i\omega_n, \boldsymbol{k})$, $p = (p_0, \boldsymbol{p})$ and $p' = (p_0, \boldsymbol{p'})$ with $p_0 = \omega(\boldsymbol{p}) = v(T)|\boldsymbol{p}| + \mathcal{O}(|\boldsymbol{p}|^3)$.

Since we are dealing with a slow process, we should enforce the mass-shell condition at the very beginning. We can take advantage of the facts that the pion is massless and that the scattering is elastic and enforce the on-shell condition by setting all external Matsubara frequencies to zero. This step is perfectly legal, because the Euclidean point $i\omega = i2\pi l$ with $l = 0$ happens to lie on the real axis and coincides with the point $\omega = 0$. Then, the calculation of the on-shell form factor from Eq. (37) involves the following steps: (1) combine the denominators using the Feynman parameter representation; (2) carry out the spatial momentum integral; (3) eliminate all momentum variables in terms of the two independent variables $\boldsymbol{q}^2$ and $\omega(\boldsymbol{p})$; (4) extract $F[\boldsymbol{q}^2, \omega(\boldsymbol{p})]$ from $f_i(p,p')$ using Eq. (35); (5) take the limit $\omega(\boldsymbol{p}) -> m_\pi$. Without going through the details, which are tedious but straightforward, we directly give the final result

$$F[\boldsymbol{q}^2, \omega(\boldsymbol{p}) \to 0] = \frac{g_\pi^2(T)}{2\pi} T \sum_{n=-\infty}^{\infty} \int_0^1 d\alpha \frac{1}{\omega_n^2 + m^2 + \alpha(1-\alpha)\boldsymbol{q}^2}\,. \tag{38}$$

The Matsubara frequency sum can be readily carried out, yielding

$$F[\boldsymbol{q}^2, \omega(\boldsymbol{p}) \to 0] = g_\pi^2(T) \frac{\tanh(m/2T)}{4\pi m} \left\{ 1 - \frac{\boldsymbol{q}^2}{12m^2} \Big[ 1 - \frac{(m/T)}{\sinh(m/T)} \Big] \right\} + \mathcal{O}(\boldsymbol{q}^4)\,. \tag{39}$$

Using the explicit expression of $g_\pi^2(T)$ in Eq. (30) we immediately find that the effective charge $F[0, \omega(\boldsymbol{p})] \leq 1$, with the equality sign only at $T = 0$. The fact that $F[\boldsymbol{q}^2, \omega(\boldsymbol{p})]$ vanishes in the limit $T \to T_c$ merely reflects the fact that the cross section for a lepton to hit the pion also vanishes in the same limit, consistent with the decoupling of the pion from its constituents at the chiral restoration point. As another consistency check, $F[0, \omega(\boldsymbol{p})]$ can also be calculated from the full pion propagator $S_\pi[\omega, \boldsymbol{p}^2]$ through the Ward identity, in the limit of $\boldsymbol{p}^2 \to 0$

$$F[0, \omega(\boldsymbol{p})] \;=\; g_\pi^2(T)\, \frac{\partial}{\partial \boldsymbol{p}^2} S_\pi^{-1}[\omega, \boldsymbol{p}^2] \bigg|_{\omega = \omega(\boldsymbol{p})}\,, \tag{40}$$

which is a consequence of the residual static gauge invariance at finite temperature. In the above equation one must use the full pion propagator in the limit of slow processes, i.e. taking $\omega = 0$ before sending $\boldsymbol{p}^2$ to zero as it was done in Eq. (25); this limit differs from the one used to produce Eq. (28) which is defined for fast processes. As we anticipated, the charge conservation that guarantees $F[0] = 1$ at $T = 0$ no longer holds at finite $T$, due to the well-known charge screening. The effective charge $F[0]$ is the pion charge plus the charge in its thermal cloud. The explicit charge conservation only can be expected in a deeply inelastic process, in which the on-shell condition is enforced at the end of the form factor calculation. Of course, the total charges of the test particle and the heat bath is definitely

conserved. However, in a slow scattering process, the lepton only sees the charges localized near the test particle, but not those charges far away at the spatial boundary.

It would be interesting to calculate directly the thermal-cloud charge distribution induced by a pion. However, this calculation appears to be beyond the scope of the linear response theory. The reason is that, according to the linear response theory, the induced thermal cloud is proportional (in momentum space) to the charge distribution of the test particle, and the temperature dependence appears only in the proportionality function, i.e. the retarded correlation function. In our case, the test particle itself has a non-trivial internal structure, which is subject to change under the thermal environment. Therefore, there is back-reaction between the induced thermal cloud and the structure of the pion, which is not an external probe. This intricate entangling of the test particle and the thermal environment necessarily prompted us to the calculation of the on-shell form factor.

Now the radius of the pion in the heat-bath frame can be obtained easily

$$\langle r^2\rangle_T = \frac{1}{3m^2}\Big[1 - \frac{m/T}{\sinh(m/T)}\Big]\,. \tag{41}$$

The complete curve of $\langle r^2\rangle_T$ as a function of $T$ is displayed in Fig. 5, which makes sense only in the symmetry broken phase where the pion exists. At zero temperature $\langle r^2\rangle_0 = 1/(3\mu^2)$, which can also be verified directly from the covariant calculation at $T = 0$, where $F[q^2] = [4m^2/(-q^2)]^{1/2}\sin^{-1}[(-q^2)/(4m^2 - q^2)]^{1/2}$, with $q^2 = q_0^2 - \boldsymbol{q}^2$. Near critical temperature $\langle r^2\rangle_T \to 1/(18T_c^2) = 2(\ln 2)^2/(9\mu^2)$. Although the pion's size decreases as temperature increases from zero to the critical point by about factor of 3, the characteristic size scale of the pion remains to be $1/\mu^2$. This is related to the fact that the pion, once it forms, is always a tightly bound state when $T < T_c$.

It is also interesting to point out that, in general, the radius $\langle r^2\rangle_T$, defined through slow processes, can not be simply estimated by the threshold of the triangle graph, which is a standard practice at $T = 0$. In fact, if one did so, one would obtain the wrong estimate $\langle r^2\rangle_T \sim 1/m^2$, which diverges when $T \to T_c$. The phase space integral, which produces the factor in the brackets in Eq. (41), can play an important role at finite temperature. As can be seen clearly from Eq. (38), the actual singularity structure of $F[\boldsymbol{q}^2, \omega(\boldsymbol{p}) \to 0]$ in $\boldsymbol{q}^2$ is always controlled by the lowest threshold $4M_1^2 \equiv 4(\pi^2T^2 + m^2)$, which stays of order $\mu^2$ in the entire broken phase. A physical interpretation can be given for Eqs. (38) and (41): the thermal environment tends to wash out coherence beyond the thermal wave length $(1/T)$ in slow processes.

At this point the physical picture is clear. At low temperature, the pion state is very much the usual pion state with exponentially small correction from the thermal environment. As temperature increases the quark and antiquark become less and less likely to bind together to form the elementary excitation. However, once they bind together, the elementary excitation remains qualitatively similar to its zero temperature counterpart. Above the critical temperature the pion completely resolves into its constituents and no longer exists. So the phase structure of the system is strongly reflected from its spectral content in Minkowski space.

In sharp contrast, the screening Bethe-Salpeter amplitude defined in the Euclidean space does not share this feature, since it is insensitive to the real-time singularity structure, as we

shall demonstrate in the next section. Nonetheless, the screening Bethe-Salpeter amplitude indeed provides a qualitative measure of the size of the corresponding bound state, though only in the phase where the bound state can be identified as an elementary excitation. This is due to the fact that the on-shell form factor and the screening Bethe-Salpeter amplitude have thresholds proportional to $M_1^2$.

Can the result in Eq (41) be an accident of the 2+1 dimensional Gross-Neveu model? To settle this question we need to study the on-shell form factor in 3+1 dimensions, i.e. in the Nambu-Jona-Lasinio model. In 3+1 dimensions, we find that the resulting formula is not very different from the one in 2+1 dimensions, Eq. (38): apart from some trivial factors, which are independent of the momentum transfer, the only modification is that the integrand of the $\alpha$-integral is raised to the power 1/2, as it is obvious from dimensional counting. Therefore, the lowest singularity in $\boldsymbol{q}^2$-plane is still given by $4M_1^2$. Although now the form factor requires a cutoff in the Matsubara frequency sum, the charge radius is independent of this cutoff. This implies that the charge radius in 3+1 dimensions has qualitatively the same behavior as in the 2+1 dimensional case. Our result, a pion charge radius that remains finite at the critical temperature both in the 2+1 Gross-Neveu model and in the 3+1 Nambu-Jona-Lasinio model, is in sharp contradiction with the result found in Ref. [12], a pion charge radius that diverges at the critical temperature in the Nambu-Jona-Lasinio model. Since the result of Ref. [12] is not expressed through a simple formula such as our Eqs. (38) and (41), but is obtained by means of a numerical integration of an expression that involves principal value definitions, we have not been able to pin down the source of this discrepancy. However, it is worth mentioning that Schulze used the temporal component of the triangle graph to define the charge radius, which we believe is less desirable due to the contamination from the second form factor $G$ associated with the heat bath. It is also not clear at what exact stage he enforced the on-shell condition, and hence it is not clear whether his form factor is defined for fast or slow processes. Either of these two points could lead to very different results and, more importantly, to different interpretations in terms of physical measurements.

### D. Spectral Function

We now calculate the spectral function in the pseudoscalar channel. We give the result for $\boldsymbol{p} = 0$, where the cut contribution near the origin, due to the scattering of the current and thermal particles, vanishes. Below $T_c$ we have a contribution from the continuum ($\omega > 2m$), and a pole contribution from the bound state:

$$\rho(\omega) = \epsilon(\omega) \left[ \pi \frac{N^2 g_\pi^2(T)}{g^4} \delta(\omega^2 - m_\pi^2) + \theta(\omega^2 - 4m^2(T))\, \rho_{\rm cont}(\omega) \right], \tag{42}$$

where the bound state mass $m_\pi = 0$, and the coupling $g_\pi^2(T)$ is given in Eq. (30). Above $T_c$ only the contribution from the continuum survives. The continuum part of the spectral function is related to the real and imaginary parts of the bubble graph, see Eqs. (23), in the following way

$$\rho_{\rm cont}(\omega) = \frac{{\rm Im}\left[i\Pi_P(\omega)\right]}{\left(1 - (g^2/N){\rm Re}\left[i\Pi_P(\omega)\right]\right)^2 + \left((g^2/N){\rm Im}\left[i\Pi_P(\omega)\right]\right)^2}. \tag{43}$$

We show the spectral function at different temperatures in Fig. 4. The most remarkable feature is that near the phase transition the shape of the spectral function is very different from its shape at low temperature. A large peak develops just above threshold. The peak actually diverges right at the phase transition, though its integrated strength stays finite. At the same time, as expected, the pole becomes weaker and the threshold goes to zero. These qualitative features are not artifacts of the particular model we are considering here. They actually are the characteristics of a continuous phase transition and critical phenomena. For example, the strong peak near the threshold is a reflection of the fact that the corresponding susceptibility diverges at $T_c$. These characteristics would still persist to a certain extent when the phase transition is weekly first order. Furthermore, as we argued in Ref. [13], QCD shares all these qualitative features.

The strong peak near the origin in the spectral function, when $T$ is close to $T_c$, indicates a resonance-like excitation. This resonance corresponds to a complex pole of the two-point function on the second Riemann sheet of the $\omega^2$-plane, with a very small imaginary part. Using explicit formulae in Sec. III, one can analytically continue the two-point function onto the second Riemann sheet. Then, it is not hard to find that the real and imaginary parts of the pole in the symmetric phase are proportional to $t/\ln(t^{-1})$ and $-t/\ln^2(t^{-1})$, respectively, where $t \equiv (T - T_c)/T_c \ll 1$. As $T$ gradually increases from $T_c$ this resonance pole moves almost parallel to the real axis from the origin to the right initially; and it eventually marches into the first quadrant. When $T$ is outside the scaling region, the imaginary part of this complex pole becomes so big such that it does not makes sense anymore to call it a resonance excitation.

It appears that the diminishing of the pion strength and the magnification of the quark-antiquark continuum strength in the spectral function near the critical region provides a possible physical picture for the failure of the standard $\sigma$-model scenario [14] in predicting the nature of the chiral-symmetry-restoration phase transition [3] in the Gross-Neveu model in 2+1 dimensions. To substantiate this statement a detailed investigation is necessary. The reason is that the $\sigma$ field in the relevant $\sigma$-model does not necessarily correspond to any real-time bound state pole, but more likely to the resonance pole mentioned above.

### E. Sum Rule

To quantitatively characterize the weakening of the pole and the growing of the peak above threshold we derive an exact sum rule for the temperature dependent part of the zeroth moment of the spectral function.

To derive the sum rule we need to find out the asymptotic behaviors of the two-point function in the deep Euclidean region and of the spectral function in the large-$\omega^2$ limit. Using the expression in Eq. (21) it is easy to obtain the pseudoscalar bubble graph in the Euclidean region

$$i\Pi_P(iQ, \boldsymbol{p} \to 0) = \frac{N}{g^2} + \frac{N}{\pi}\Big\{R(T) - \frac{Q}{2}\tan^{-1}\frac{Q}{2m} + \frac{Q^2}{4}\int_m^\infty dE\,\frac{2}{1+e^{E/T}}\,\frac{1}{E^2+Q^2/4}\Big\}\,, \quad (44)$$

and its asymptotic form at large-$Q^2$

$$\frac{1}{N} i\Pi_P(iQ, \boldsymbol{p} \to 0) \sim -\frac{Q}{4} + \Big(\frac{1}{g^2} + \frac{\mu}{\pi}\Big) - \frac{4}{3\pi}\,\frac{m^3 + 3\langle\!\langle E^2 \rangle\!\rangle}{Q^2} + \mathcal{O}(Q^{-4})\,, \tag{45}$$

where $\langle\!\langle \cdots \rangle\!\rangle$ stands for the thermal average

$$\langle\!\langle A \rangle\!\rangle \equiv \int_m^\infty dE\, \frac{2}{1 + e^{E/T}}\, A(E)\,. \tag{46}$$

For example, $\langle\!\langle E^2 \rangle\!\rangle = 3\zeta(3)T^3$, in the symmetric phase where $m = 0$. The corresponding two-point function, defined in Eq. (26), is

$$\langle J_5 J_5 \rangle_T(iQ, 0) \sim -\frac{N}{g^2}\Big\{1 - \frac{4}{g^2 Q}\Big[1 + \frac{4\mu}{\pi Q} + \frac{16\mu^2}{\pi^2 Q^2} + \frac{64\mu^3 - 16\pi^2(m^3 + 3\langle\!\langle E^2 \rangle\!\rangle)/3}{\pi^3 Q^3}\Big]\Big\} + \mathcal{O}(Q^{-5})\,. \tag{47}$$

On the other hand, the spectral function has the following asymptotic form at large $\omega^2$, as can be derived from Eqs. (23) and (43),

$$\rho(\omega) \sim \frac{4N}{g^4 \omega}\Big\{1 - 16\Big(\frac{\mu - R(T)}{\pi\omega}\Big)^2\Big\} + \mathcal{O}(\omega^{-5})\,. \tag{48}$$

To study the temperature dependence we make the subtraction, following Ref. [13],

$$\Delta\langle J_5 J_5 \rangle(iQ, 0) \equiv \langle J_5 J_5 \rangle_T(iQ, 0) - \langle J_5 J_5 \rangle_{T'}(iQ, 0) = \int_0^\infty d\omega^2 \frac{\Delta\rho(\omega)}{\omega^2 + Q^2}\,, \tag{49}$$

with $\Delta\rho(\omega) \equiv \rho_T(\omega) - \rho_{T'}(\omega)$. Since the leading term in $\rho_T(\omega)$ is independent of $T$, as seen from Eq. (48), we immediately have $\Delta\rho \sim \omega^{-3}$. This implies that the zeroth moment of $\Delta\rho$ exists. Using Eq. (47), and hence

$$\Delta\langle J_5 J_5 \rangle(iQ, 0) \sim \frac{64N}{3\pi g^4}\,\frac{\Delta(m^3 + 3\langle\!\langle E^2 \rangle\!\rangle)}{Q^4} + \mathcal{O}(Q^{-5})\,, \tag{50}$$

we arrive at the following expression appropriate to derive the sum rule

$$\frac{64N}{3\pi g^4}\,\frac{\Delta(m^3 + 3\langle\!\langle E^2 \rangle\!\rangle)}{Q^2} = \int_0^\infty d\omega^2 \frac{\Delta\rho}{1 + \omega^2/Q^2} + \mathcal{O}(Q^{-3})\,, \tag{51}$$

where $\Delta(m^3 + 3\langle\!\langle E^2 \rangle\!\rangle) \equiv (m^3 + 3\langle\!\langle E^2 \rangle\!\rangle)_T - (m^3 + 3\langle\!\langle E^2 \rangle\!\rangle)_{T'}$. Taking the limit $Q^2 \to \infty$ we get the desired sum rule

$$\int_0^\infty d\omega^2\, \Delta\rho = 0\,, \tag{52}$$

Interchanging the order of the dispersion integral and the $Q^2 \to \infty$ limit is allowed since the zeroth moment is finite.

We have proved that the very same sum rule also holds in the 1+1 dimensional Gross-Neveu model and QCD [13], though we have used a totally different derivation in those cases and the corresponding sum rules would only converge logarithmically. It appears that

the temperature dependence of the zeroth moment of the spectral function often shows qualitatively similar behaviors, no matter what is the underlying microscopic physics.

Another interesting point, which was especially clear in the derivation we used for the 1+1 dimensional Gross-Neveu model and QCD [13], is that the zeroth moment of the spectral function could be related, in asymptotically free theories, to expectation values of appropriate operators via the operator product expansion. That result cannot be immediately applied to the 2+1 Gross-Neveu model, since this model is not asymptotically free and possesses a nontrivial ultra-violet fixed point. Therefore, it would be extremely interesting to investigate whether a formalism similar to the operator product expansion [15] can be extended to this case.

## V. SCREENING PHENOMENA

As discussed in section II, screening phenomena are associated with responses to time-independent external perturbations. Therefore, we only need to consider static Green's functions and purely spatial correlation functions. Static Green's functions are essentially Euclidean and hence, in contrast to the time-dependent responses we have discussed in the preceding section, well-suited for the lattice formulation. In this section we study the static two-point and three-point functions that relate to screening masses and screening Bethe-Salpeter amplitudes, respectively, since these quantities are studied on the lattice [5,6].

### A. Screening mass

The pseudoscalar screening mass $\tilde{m}$ is the lowest solution to the equation

$$0 = 1 - \frac{g^2}{N}\Pi_P(i\omega \to 0, i\boldsymbol{p}) = -\frac{g^2}{\pi}\left\{ R(T) + 2T \sum_{n=-\infty}^{\infty} \sqrt{\frac{\boldsymbol{p}^2}{4M_n^2 - \boldsymbol{p}^2}}\, \tan^{-1}\sqrt{\frac{\boldsymbol{p}^2}{4M_n^2 - \boldsymbol{p}^2}} \right\} . \tag{53}$$

When $R(T) = 0$ ($T < T_c$), the solution is obvious: $\boldsymbol{p}^2 = 0 = \tilde{m}_\pi^2$. In the high temperature phase $R(T) \neq 0$, the solution can only be obtained numerically.

Contrary to the naive expectation that higher than lowest Matsubara modes decouple at high $T$, we point out that the frequency sum in Eq. (53) cannot be truncated without introducing an error in the screening mass that is not of order $1/T$. This fact suggests that dimensional reduction does not take place in this model [16]. Details on this point will be presented later.

We can define a coupling constant for the screening state analogous to the one defined for the real-time bound state case

$$\tilde{g}_\pi^2(T) = \left( \frac{\partial}{\partial \boldsymbol{p}^2}\Pi_P(i\omega \to 0, \boldsymbol{p}) \right)^{-1}_{\boldsymbol{p}^2 = -\tilde{m}_\pi^2} . \tag{54}$$

Then, near the screening-mass pole, the static pseudoscalar propagator behaves like $\tilde{g}_\pi^2(T)/(\boldsymbol{p}^2 + \tilde{m}_\pi^2)$. In Fig. 2 $\tilde{g}_\pi^2(T)$ is plotted in dashed line. Even though $\tilde{g}_\pi^2$ agrees with

$g_\pi^2$ at $T=0$, due to the Euclidean invariance, it becomes drastically different from $g_\pi^2$ as temperature increases. In particular, $\tilde{g}_\pi^2$ does not vanish in the symmetric phase, but rather grows linearly with $T$ in the high-$T$ limit. In the broken phase $\tilde{g}_\pi^2(T)$ has a particularly simple form: $\tilde{g}_\pi^2(T) = 4\pi m/[N\,\tanh(m/2T)]$.

As in the real-time case, an analogous "decay constant" for the "on-shell" screening pion can be defined. Again it is easy to verify

$$\tilde{f}_\pi(T) = \tilde{g}_\pi(T)\,\frac{N}{2\pi}\,\tanh\left(\frac{m(T)}{2T}\right)\,, \tag{55}$$

which also vanishes in the symmetric phase. It is interesting to notice that the "Goldberger-Treiman" relation holds exactly in the screening case

$$\tilde{g}_\pi(T)\,\tilde{f}_\pi(T) = 2m(T)\,. \tag{56}$$

We believe that this result is not accidental, because the screening state in the static limit can be regarded as a bound state in some 1+1 dimensional theory at zero temperature with the same symmetry as the original theory. This Euclidean "Goldberger-Treiman" relation is in agreement with the results of Ref. [11].

In order to explicitly see the manifestation of the chiral symmetry also in the screening masses, it is instructive to calculate the scalar screening mass. The scalar bubble graph (in the static limit) is easily related to the pseudoscalar counterpart

$$\Pi_S(i\omega\to 0,\boldsymbol{p}) = \Pi_P(i\omega\to 0,\boldsymbol{p}) - \frac{NT}{\pi}\sum_{n=-\infty}^{\infty}\frac{4m^2}{\boldsymbol{p}^2}\sqrt{\frac{\boldsymbol{p}^2}{4M_n^2+\boldsymbol{p}^2}}\,\ln\left[\frac{\sqrt{4M_n^2+\boldsymbol{p}^2}+\sqrt{\boldsymbol{p}^2}}{\sqrt{4M_n^2+\boldsymbol{p}^2}-\sqrt{\boldsymbol{p}^2}}\right]\,. \tag{57}$$

Similarly to the pseudoscalar screening mass, the scalar screening mass is found by solving the equation

$$\begin{aligned} 0 &= 1 - \frac{g^2}{N}\Pi_S(i\omega\to 0, i\boldsymbol{p}) \\ &= -\frac{g^2}{\pi}\left\{R(T) + 2T\sum_{n=-\infty}^{\infty}\frac{\boldsymbol{p}^2-4m^2}{\boldsymbol{p}^2}\sqrt{\frac{\boldsymbol{p}^2}{4M_n^2-\boldsymbol{p}^2}}\,\tan^{-1}\sqrt{\frac{\boldsymbol{p}^2}{4M_n^2-\boldsymbol{p}^2}}\right\}\,. \end{aligned} \tag{58}$$

When $T<T_c$, $R(T)=0$ and the solution is again easily obtained $\boldsymbol{p}^2 = 4m^2 = \tilde{m}_\sigma^2$ (notice that $\boldsymbol{p}^2=0$ is not a solution in this channel). For $T>T_c$ the dynamical quark mass $m^2(T)$ vanishes, and the scalar screening mass equation becomes identical to the one for the pseudoscalar screening mass.

In Fig. 6 we display numerical results for the screening masses in both channels, pseudoscalar and scalar. In the low temperature phase, chiral symmetry is broken, and the pion is the relevant Goldstone boson: this fact is also reflected in the screening mass. In the high temperature phase, chiral symmetry is restored, and we find the expected parity doubling, i.e. the degeneracy of the screening masses in the parity mirrored channels.

We already know that the screening state is very different from the real-time bound state. One might, however, naturally ask whether the screening state be somehow related

to the resonance excitation near $T_c$. In particular, one might want to introduce some non-trivial external momentum dependence in the screening state and hope that, by making this external spatial momentum complex, the screening pole might be continued into the resonance pole. While this option is in principle possible, we think that a more relevant question is whether the knowledge of the static screening state as a function of temperature is sufficient by itself, i.e. when we do not have complete knowledge of the analytic structure of the two-point function, to provide enough direct information on the resonance state. We think that the answer to this latter question is unlikely to be affirmative. The reason is that the functional dependences of the two-point function on frequency and spatial momemtum at finite $T$ are genuinely different, due to the explicit lack of Lorentz invariance. Therefore, it is not possible to probe, in general, the full information carried by the frequency variable by varying a spatial component of the momentum. In addition, the following three points also support this general view. First, the screening pole is purely imaginary for any $T$, whereas the resonance pole is complex in general. Second, the screening state is well defined for any $T$, whereas the resonance is only identifiable near the critical region. The third point is more specific to the model we have consider: when $T \gtrsim T_c$, the screening mass squared is proportional to $t$, with $t = (T - T_c)/T_c \ll 1$, whereas the resonance pole is proportional to $t$ with logarithmic corrections (see section IV.D).

### B. Screening Bethe-Salpeter amplitude

Another observable that is calculated on the lattice at finite temperature [6] is the screening Bethe-Salpeter amplitude (SBSA). Our definition of this amplitude in the pseudoscalar channel is

$$\phi(x,y) \equiv \int d\tau\, dz\, \langle \bar{\psi}(\tau,x,z)\gamma_5\psi(\tau,x,z+y)\, \bar{\psi}(0,0,0)\gamma_5\psi(0,0,0)\rangle\,. \tag{59}$$

This definition differs from the usual lattice definition by an extra integration over $\tau$. We perform this extra integration for computational convenience, since it allows us to consider only the zero frequency mode. In terms of physical content of the SBSA, this difference should be irrelevant. To the leading order in $1/N$, the Feynman graphs contributing to the SBSA are those shown in Fig. 7. Then the Fourier transform of $\phi(\tau, y)$ has the following form

$$\tilde{\phi}(p_1,p_2) = \frac{\tilde{\phi}_1(p_1,p_2)}{1 - g^2\Pi_P(i\omega \to 0, \boldsymbol{p} = (p_1,0))/N}\,, \tag{60}$$

where $\tilde{\phi}_1(p_1,p_2)$ is the off-shell screening BS amplitude

$$\tilde{\phi}_1(p_1,p_2) = iNT\sum_n \int \frac{d^2\boldsymbol{k}}{(2\pi)^2}\mathrm{Tr}\left[i\gamma_5\,\frac{i}{k\cdot\gamma - m}\,i\gamma_5\,\frac{i}{k\cdot\gamma - p\cdot\gamma - m}\right]_{p=(i\omega\to 0,p_1,p_2)}\,. \tag{61}$$

An explicit calculation yields

$$\tilde{\phi}_1(p_1,p_2) = 2NT\sum_{n=-\infty}^{\infty}\frac{\sqrt{M_n^2 + p_2^2}}{M_n^2 + p_2^2 + p_1^2/4}\,. \tag{62}$$

Therefore, the complete SBSA is

$$\phi(x,y) = \int \frac{dp_2}{2\pi}\, e^{-ip_2 y} \int \frac{dp_1}{2\pi}\, e^{-ip_1 x} \frac{\tilde{\phi}_1(p_1,p_2)}{1 - g^2 \Pi_P(p = (i\omega \to 0, p_1, 0))/N}\,. \tag{63}$$

Typically, we are interested in the dependence of the SBSA on $y$ for large $x$, so that we project on the lowest "screening state". In the limit $x \to \infty$ the $p_1$–integral picks out the lowest singularity, $p_1^2 = \tilde{m}_\pi^2 < 4M_n^2$, and the SBSA becomes

$$\phi(x,y)\Big|_{x\to\infty} \longrightarrow \frac{\tilde{g}_\pi^2 N}{2\tilde{m}_\pi}\, e^{-\tilde{m}_\pi x} \sum_{n=-\infty}^{\infty} 2T \int \frac{dp_2}{2\pi}\, e^{-ip_2 y} \frac{\sqrt{M_n^2 + p_2^2}}{M_n^2 - \tilde{m}_\pi^2/4 + p_2^2}\,. \tag{64}$$

The scale that controls the size of the screening wave function is clearly $\sqrt{M_1^2 - \tilde{m}_\pi^2/4}$, as one can show by deforming the integration contour to the imaginary axis. Since $M_1^2 = (\pi T)^2 + m^2$, and $m_\pi = 0$ at low temperature, in the low $T$ limit this scale is $m \propto \mu$. At high temperature $m = 0$, and $m_\pi \propto T$, therefore in this limit the scale is set by $\sqrt{\pi^2 T^2 - \tilde{m}_\pi^2/4} \sim T$.

As we have argued in the preceding section, a better measure of the spatial distribution of the quark and antiquark inside a meson is provided by its on-shell form factor. The SBSA qualitatively measures the size of the elementary excitation, or bound state, in the entire broken phase. However, the SBSA above the phase transition does not yield any information about the nature of the corresponding (nonexistent) real-time bound state.

We also calculate the SBSA in the scalar channel using exactly the same procedure we have used in the pseudoscalar channel, and we find very similar results. The relevant mass scale is now given by $\sqrt{M_1^2 - \tilde{m}_\sigma^2/4}$, which has the same high temperature limit as the scale for the pseudoscalar channel. In the broken phase ($T < T_c$), since $\tilde{m}_\sigma^2 = 2m$, and $M_1^2 = (\pi T)^2 + m^2$, $\sqrt{M_1^2 - \tilde{m}_\sigma^2/4} = \pi T$. This last result is consistent with the fact that there is no binding energy in the scalar channel, and the only screening is due to the thermal mass.

### C. Real-time vs. screening phenomena

Now we have all the ingredients to make an explicit comparison between the real-time bound state and the screening state.

*Mass*: When $T < T_c$ (the chiral symmetry is spontaneously broken), both the real-time and the screening pion masses vanish, $m_\pi(T) = \tilde{m}_\pi(T) = 0$, while the scalar mass $\tilde{m}_\sigma(T) = 2m(T)$. However, when $T > T_c$ (chirally symmetric phase), the real-time pion decouples and the spectral function has contributions only from the quark-antiquark continuum, whereas the screening pion mass $\tilde{m}_\pi(T)$ becomes degenerate with the screening scalar mass $\tilde{m}_\sigma(T)$ and both of them asymptotically grow linearly with $T$ (see Fig. 6).

*Coupling*: The real-time coupling of the pion to the quark-antiquark state, $g_\pi^2(T)$, and the corresponding screening coupling, $\tilde{g}_\pi^2(T)$, have very different behaviors as functions of temperature, as it is clearly shown in Fig. 2, and they only coincide at $T = 0$. In particular, the screening coupling $\tilde{g}_\pi^2(T)$ does not provide any signal for the fact that the real-time

excitation decouples when $T \geq T_c$; in fact $\tilde{g}_\pi^2(T)$ does not show any distinctive feature near the critical region.

*Decay constant*: Both $f_\pi(T)$ and $\tilde{f}_\pi(T)$ start at the same value at $T = 0$ and gradually decrease to zero at $T = T_c$. The vanishing of $f_\pi(T)$ and $\tilde{f}_\pi(T)$ when $T \geq T_c$ is due to the fact that the axial current decouples from the pseudoscalar current when the chiral symmetry is restored. This constraint forces a similar behavior for both $f_\pi(T)$ and $\tilde{f}_\pi(T)$, even if their numerical values between $T = 0$ and $T = T_c$ are different. Above the phase transition, $f_\pi$ loses its meaning, and $\tilde{f}_\pi(T)$ remains zero.

*Size*: As seen from Fig. 5, the sizes defined through the on-shell form factor in the elastic limit, $\langle r^2 \rangle_T$ and the screening Bethe-Salpeter amplitude, $1/M_1^2$, have qualitatively similar behaviors in the broken phase. The reason for this similarity is that they share the same singularity structure in low spatial momentum transfer. Nevertheless, we find again that, while $\langle r^2 \rangle_T$ loses its meaning above $T_c$, the size defined through the screening Bethe-Salpeter amplitude does not give us any signal of this disappearance of the real-time state.

We believe that most of the above-mentioned qualitative features will also be present in 3+1 dimensions, although some of the details presented here are certainly specific to this model. Therefore, we can safely conclude that the screening observables, in general, do not necessarily reflect the behavior of the corresponding real-time observables. These two kinds of observables are often qualitatively different.

### D. High-$T$ limit and dimensional reduction

The present model study can also offer us very interesting information about the possibility of dimensional reduction for screening Green functions at high temperature.

In the symmetric phase, equations (53) and (58) coincide and can be rewritten as

$$\frac{\mu}{T_c} - \frac{\mu}{T} = 4 \sum_{n=1}^{\infty} \frac{x}{\sqrt{4(2n-1)^2 - x^2}} \tan^{-1} \frac{x}{\sqrt{4(2n-1)^2 - x^2}}\,, \tag{65}$$

where $x^2 \equiv \boldsymbol{p}^2/(\pi T)^2$. In the high-$T$ limit we can solve the above equation iteratively by setting $x = \sum_{i=0}^{\infty} c_i \, (\mu/\pi T)^i$. In particular, the first two coefficients can be easily found by solving

$$\frac{\mu}{T_c} = 4 \sum_{n=1}^{\infty} \frac{c_0}{\sqrt{4(2n-1)^2 - c_0^2}} \tan^{-1} \frac{c_0}{\sqrt{4(2n-1)^2 - c_0^2}}\,, \tag{66}$$

and

$$\frac{\mu}{c_1} = -\frac{4}{\pi} \sum_{n=1}^{\infty} \left\{ \frac{c_0}{4(2n-1)^2 - c_0^2} + \frac{4(2n-1)^2}{[4(2n-1)^2 - c_0^2]^{3/2}} \tan^{-1} \frac{c_0}{\sqrt{4(2n-1)^2 - c_0^2}} \right\}. \tag{67}$$

Therefore, the asymptotic form for the screening masses in the high-$T$ limit is,

$$\tilde{m}_{\pi,\sigma} = c_0 \, \pi T + c_1 \, \mu + \mathcal{O}(\mu/T)\,. \tag{68}$$

Numerically, $c_0 \approx 0.982$ and $c_1 \approx -0.947$. Eq. (68) is plotted in dashed line in Fig. 6. A salient feature of this asymptotic behavior is that the high temperature limit of the screening mass is $c_0\,\pi T$, where the numerical value of $c_0$ has contributions from all the Matsubara frequency. If dimensional reduction took place in the high-$T$ limit, we would find that only the lowest (or at most a finite number) modes would contribute to $c_0$. In fact, any truncation in the frequency sum in Eq. (53), and then in Eq. (66), would give a different $c_0$: the resulting error in the screening mass would not be suppressed in the high-$T$ limit.

The reason for the failure of the dimensional reduction picture is that the 2+1 dimensional Gross-Neveu model lacks the necessary scale hierarchy: there is no elementary bosonic particle whose zero mode could dominate over other modes of order $T$, and the coupling constant cannot provide a second lower scale compared to $T$, as it happens in asymptotically free theory [16], since this model has a nontrivial ultraviolet fixed point. In fact, the high-momentum behavior of the dimensionless coupling $G(\kappa) \equiv \kappa g^2(\kappa)$ has the form $G^*/(1-\mu/\kappa)$, with $G^* = \pi$ (the value of $G^*$ is scheme dependent). This nontrivial fixed point implies that this dimensionless coupling "runs", in the high temperature limit, to a finite value (since $\kappa \sim T$ [16]). Therefore the effective interaction strength at high $T$ between all the Matsubara modes ($\sim TG(T)$, once the fields have been appropriately re-scaled) is strong and its strength in units of $T$ becomes independent of temperature ($\approx TG^*$).

In this regard the Gross-Neveu model in 1+1 dimensions is very different from the one in 2+1 dimensions. The 1+1 dimensional model is asymptotically free and $g^2(T)$ runs to zero logarithmically, providing the scale hierarchy between $T$ and $g^2(T)T$ [16]. In this model dimensional reduction takes place and screening quantities are well reproduced by the lowest modes that are weakly interacting: the leading contribution to the screening mass is given by the free theory, $c_0 = 2$, the first correction to this non-interacting behavior is of the order $g^2(T)$ and it is correctly reproduced by the reduced theory. Since $g^2(T)$ runs to zero the reduced theory becomes exact asymptotically.

Finally, we should point out that the concept of dimensional reduction that we have discussed in this subsection and in Refs. [16,17], is different from the concept of dimensional reduction employed for predicting the nature of phase transitions at finite $T$ in the $\sigma$-model scenario [14]. Our criterion for dimensional reduction is more stringent and applies to a different temperature regime. We require that the static Green's functions of the original theory at high-$T$ limit be matched by the corresponding Green's functions in the reduced theory to a given accuracy, whereas in the $\sigma$-model scenario one requires that the reduced theory be able to match the thermodynamical singularities near the critical region and hence give the same critical exponents. Therefore, the success/failure of one of the two dimensional reduction pictures does not directly implies the success/failure of the other.

## VI. CONCLUSION

We have shown in a specific example, the Gross-Neveu model in 2+1 dimensions, that the direct connection between the real-time bound state and the corresponding screening state is lost at finite temperature in general, especially near and above phase transition.

In particular, the real-time pion disappears after the phase transition, as it is signaled by the vanishing of its bounding energy and of the coupling to its constituents $g_\pi^2(T)$. In spite of

this, the corresponding screening state is still strongly "bound" in the high temperature limit, and the screening coupling $\tilde{g}_\pi^2(T)$ grows linearly with $T$. The screening mass approaches the asymptotic value of $0.982\pi T$, which is much smaller than the sum of the masses of two noninteracting fermions, $2\pi T$.

Moreover, the screening Bethe-Salpeter amplitude yields sizes of order $1/T$ both in the scalar and pseudoscalar channels at high $T$, when the real-time bound state no longer exists. Therefore, no relevant information about the nature of the real-time pion can be inferred from this screening amplitude. On the contrary, we can give a natural definition of the size of the real-time pion (below the phase transition) by means of the on-shell form factor in the elastic limit, since the on-shell form factor has direct information of the relevant coupling $g_\pi^2(T)$. Furthermore, we show that the associated size cannot be estimated solely from simple threshold considerations, reflecting the fact that the thermal environment tends to wash out coherence beyond thermal wavelength in slow (compared to the equilibration time of the thermal bath) processes.

We have also computed the exact pseudoscalar spectral function of this model. The most important features of this spectral function are the diminishing of the strength of the pion pole and the magnification of the strength of the quark-antiquark continuum near the phase transition. In addition, we have derived an exact sum rule for this spectral function: the integrated strength of the spectral function is independent of $T$.

Many of the features of the 2+1 dimensional Gross-Neveu model that we have listed above are dominated by the chiral symmetry and should have their analogues in the real world. For instance, very similar results were found in the 1+1 dimensional Gross-Neveu model [13], and in the Nambu-Jona-Lasinio model [7] in 3+1 dimensions. On the other hand, certain specific aspects certainly depend on the details of the theory. For example, we find that the 2+1 dimensional Gross-Neveu model does not undergo dimensional reduction in the high-$T$ limit. But the possibility of using a lower dimensional theory to describe static correlations of the original theory when $T$ is large is strictly tied to the short distance behavior, which is very different in this model from the one in QCD [17].

Finally, we also find that it is instructive to classify physical processes according to their characteristic time scales relative to the time scale required by the thermal environment to respond to an external perturbation. We have explicitly illustrated, in the cases of the Goldberger-Treiman relation and of the effective charge of the pion, that conservation laws due to internal symmetries are manifest only in fast processes but not in slow ones.

It is our hope that all the lessons learned from this exactly soluble model study will provide some useful insights to QCD.

## ACKNOWLEDGMENTS

It is our pleasure to thank A. Kocic and J. Kogut for their valuable comments on the manuscript, for bringing several relevant references to our attention and for very instructive discussions on topics related to this work. We would also like to thank T. Hatsuda and A. Ukawa for several useful discussions. One of us (ML) gratefully thanks the Department of Energy's Institute for Nuclear Theory at the University of Washington, where this work was initiated, for their hospitality and partial support during the workshop on "Phenomenology

and Lattice QCD". This work was supported in part by funds provided by the U.S. Department of Energy (DOE) under contract number DE-FG06-88ER40427 and cooperative agreement DE-FC02-94ER40818.

# REFERENCES

* E-mail: shuang@mitlns.mit.edu and lissia@vaxca.ca.infn.it
† Present address.

[1] N. P. Landsman and Ch. G. van Weert, Phys. Rep. **145**, 141 (1987).
[2] Gross and Neveu, Phys. Rev. D **10**, 3235 (1974); B. Rosenstein, B. J. Warr and S. H. Park, Phys. Rep. **205**, 59 (1991).
[3] A. Kocic and J. Kogut, Phys. Rev. Lett. **74**, 3109 (1995); Physics e-Print archive hep-lat/9507012 (1995).
[4] A. Barducci *et al.*, Physics e-Print archive hep-ph/9507390 (1995).
[5] T. A. DeGrand and C. E. DeTar, Phys. Rev. D **34**, 2469 (1986); C. E. DeTar and J. Kogut, Phys. Rev. Lett. **59**, 399 (1987); S. Gottlieb *et al.*, Phys. Rev. Lett. **59**, 1881 (1987); Y. Koike, M. Fukugita and A. Ukawa, Phys. Lett. B **213**, 497 (1988); K. M. Bitar *et al.*, Phys. Rev. D **43**, 2396 (1991); K. D. Born *et al.*, Phys. Rev. Lett. **67**, 302 (1991);
[6] C. Bernard *et al.*, Phys. Rev. Lett. **68**, 2125 (1992); T. H. Hansson and I. Zahed, Nucl. Phys. **B374**, 227 (1992); V. Koch, E. V. Shuryak, G. E. Brown and A. D. Jackson, Phys. Rev. D **46**, 3169 (1992); S. Schramm and M. -C. Chu, Phys. Rev. D **48**, 2279 (1993).
[7] T. Hatsuda and T. Kunihiro, Phys. Rep. **247**, 221 (1994).
[8] A. L. Fetter and J. D. Walecka, "*Quantum Theory of Many-Particle Systems*, (McGraw-Hill, 1971); J. W. Negele and H. Orland, "*Quantum Many-Particle Systems*", (Addision-Wesley, Reading, PA, 1988).
[9] S. Huang, Phys. Rev. D **47**, 653 (1993).
[10] L. Dolan and R. Jackiw, Phys. Rev. D **9**, 3320 (1974).
[11] K. Shen and Z. Qiu, Phys. Rev. D **48**, 1801 (1993).
[12] H-J Schulze, J. Phys. G **20**, 531 (1994).
[13] S. Huang and M. Lissia, Phys. Lett. B **348**, 571 (1995); Phys. Rev. D **52**, 1134 (1995).
[14] R. Pisarski and F. Wilczek, Phys. Rev. D **29**, 338 (1983).
[15] Y. Kikukawa and K. Yamawaki, Phys. Lett. B **234**, 497 (1990).
[16] S. Huang and M. Lissia, Phys. Lett. B **349**, 484 (1995).
[17] S. Huang and M. Lissia, Physics e-Print archive hep-ph/9511383 (1995).

## FIGURES

FIG. 1. The dynamical mass as a function of temperature. The mass and $T$ are in units of $\mu$, which is the dynamical mass at $T = 0$.

FIG. 2. The bound state coupling constant, $g_\pi^2(T)$, as a function of temperature (solid line). The dashed line is the coupling constant for the screening state $\tilde{g}_\pi^2(T)$. Both couplings are in units of their zero temperature value: $4\pi\mu/N$.

FIG. 3. The spectral function in the pseudoscalar channel at $\boldsymbol{k} = 0$ as a function of $\omega/\mu$: (a) in the broken phase at $T = 0$ (dashed line) and $T = 0.9524\,T_c$ (solid line); and (b) in the symmetric phase at $T = 1.25\,T_c$ (solid line) and $T = 2.5\,T_c$ (dashed line). The arrows in (a) denote the pion poles at $\omega = 0$, with a slight displacement for visual clarity. The height of the arrows indicates the relative strengths of the poles.

FIG. 4. Feynman graph for the three-point function, whose on-shell value gives the form factor. The thick external lines are the pion lines and the wiggle line is the photon line.

FIG. 5. On-shell charge radius, normalized to its value at $T = 0$, $\langle r^2\rangle_T/\langle r^2\rangle_0$, as a function of temperature in the symmetry broken phase. For comparison, the "size" estimated from the screening Bethe-Salpeter amplitude, $1/M_1^2$, is also plotted in dashed line.

FIG. 6. Screening masses in the scalar ($\sigma$) and pseudoscalar ($\pi$) channels in units of $\mu$. It is also plotted in dashed line the asymptotic formula at high-$T$ limit, $\tilde{m}_\sigma = \tilde{m}_\pi = 0.982\,\pi T - 0.947\mu$.

FIG. 7. Feynman graphs for the screening Bethe-Salpeter amplitude.

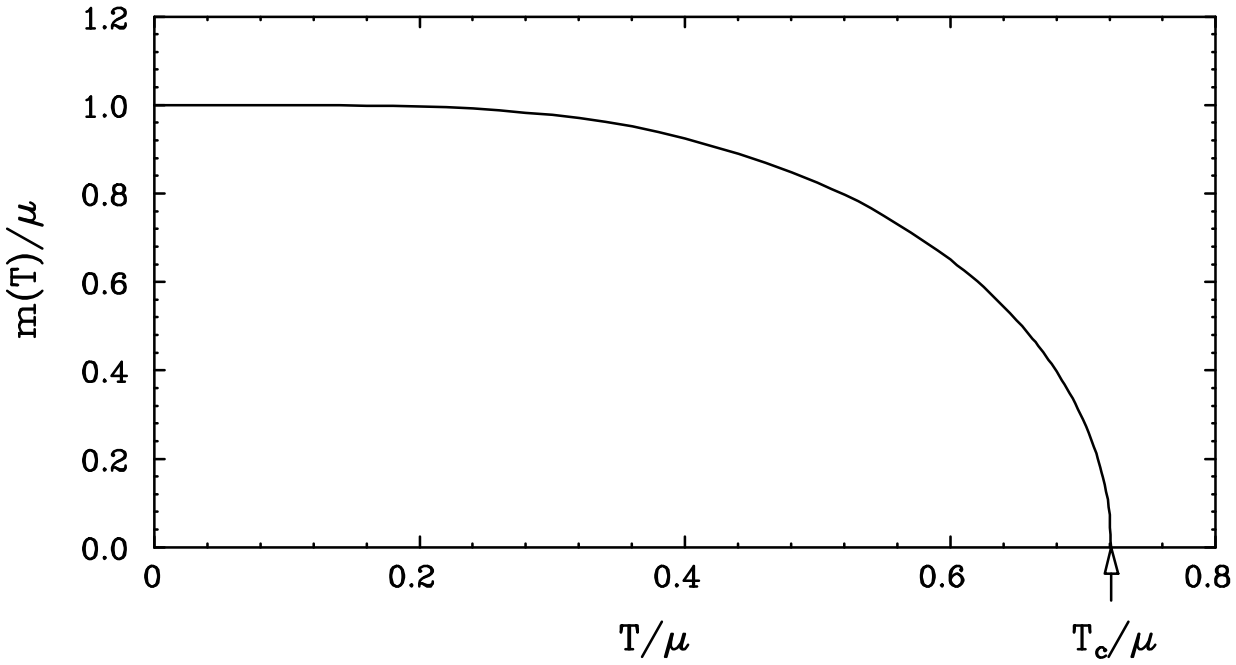


Figure 1

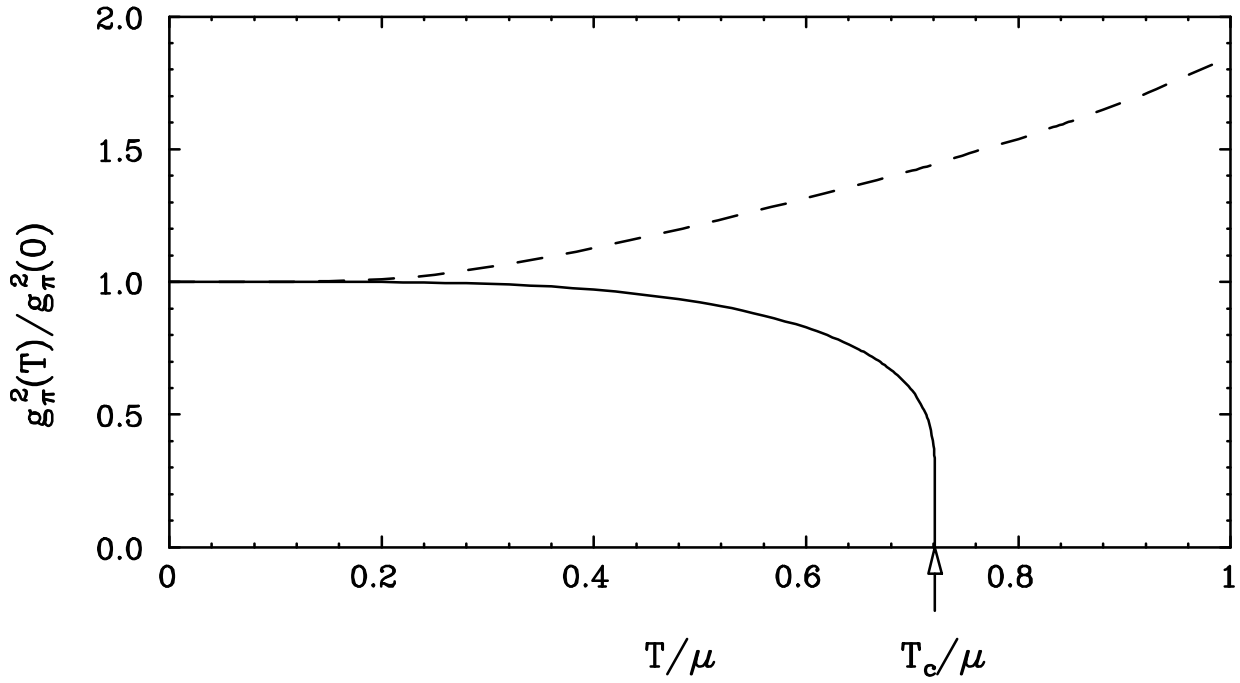


Figure 2

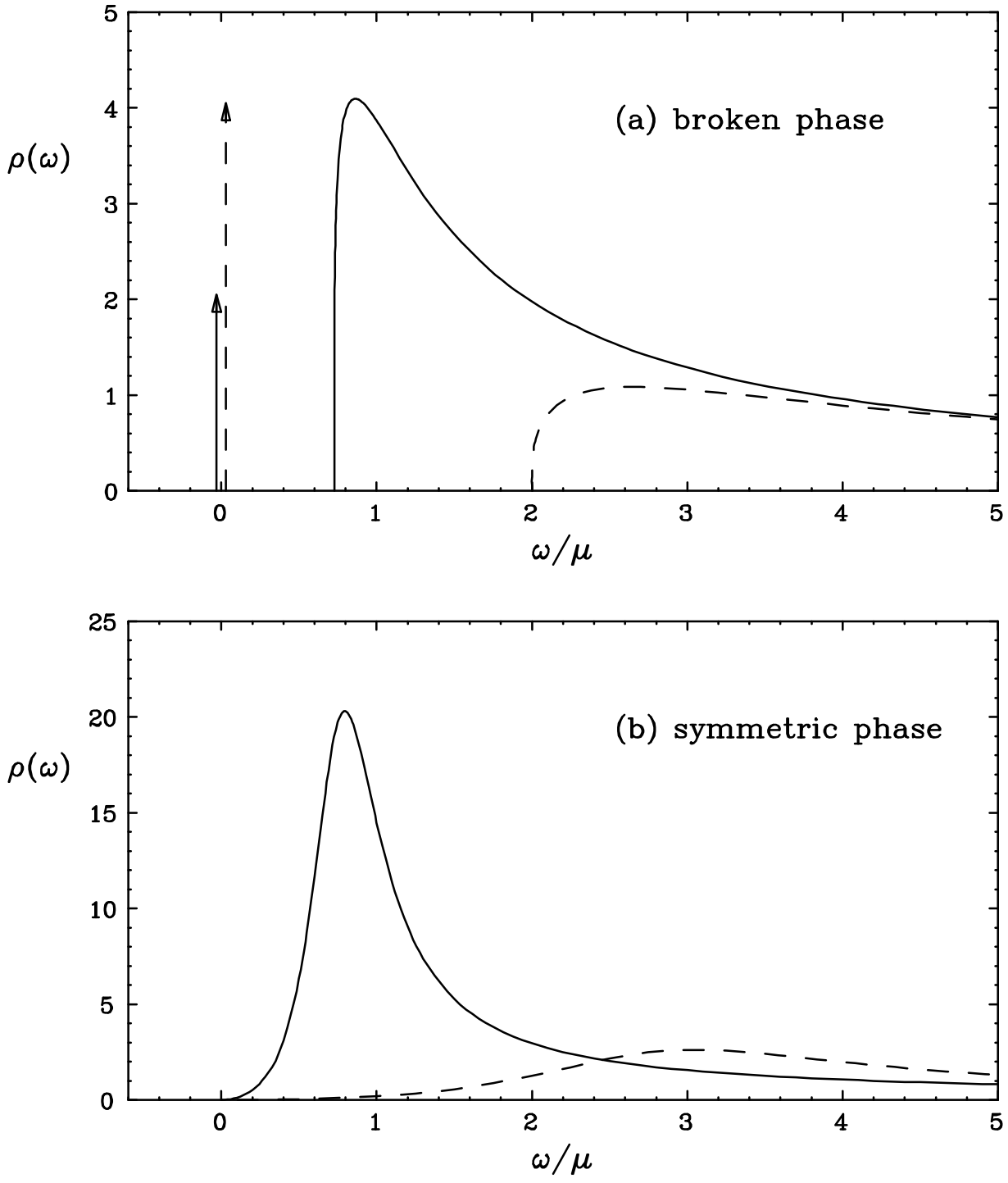
(a) broken phase
ρ(ω)
ω/μ
0
1
2
3
4
5
(b) symmetric phase
ρ(ω)
ω/μ
0
5
10
15
20
25

Figure 3

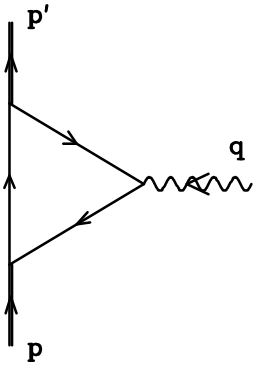


Figure 4

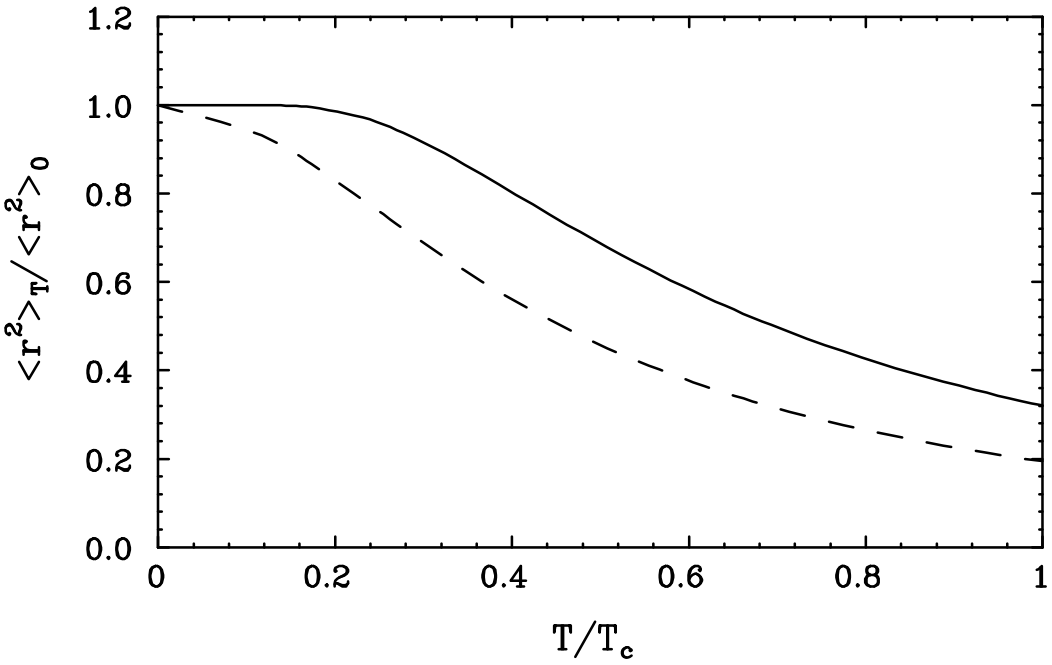
1.2
1.0
0.8
0.6
0.4
0.2
0.0
0
0.2
0.4
0.6
0.8
1
$\langle r^2\rangle_T/\langle r^2\rangle_0$
$T/T_c$

Figure 5

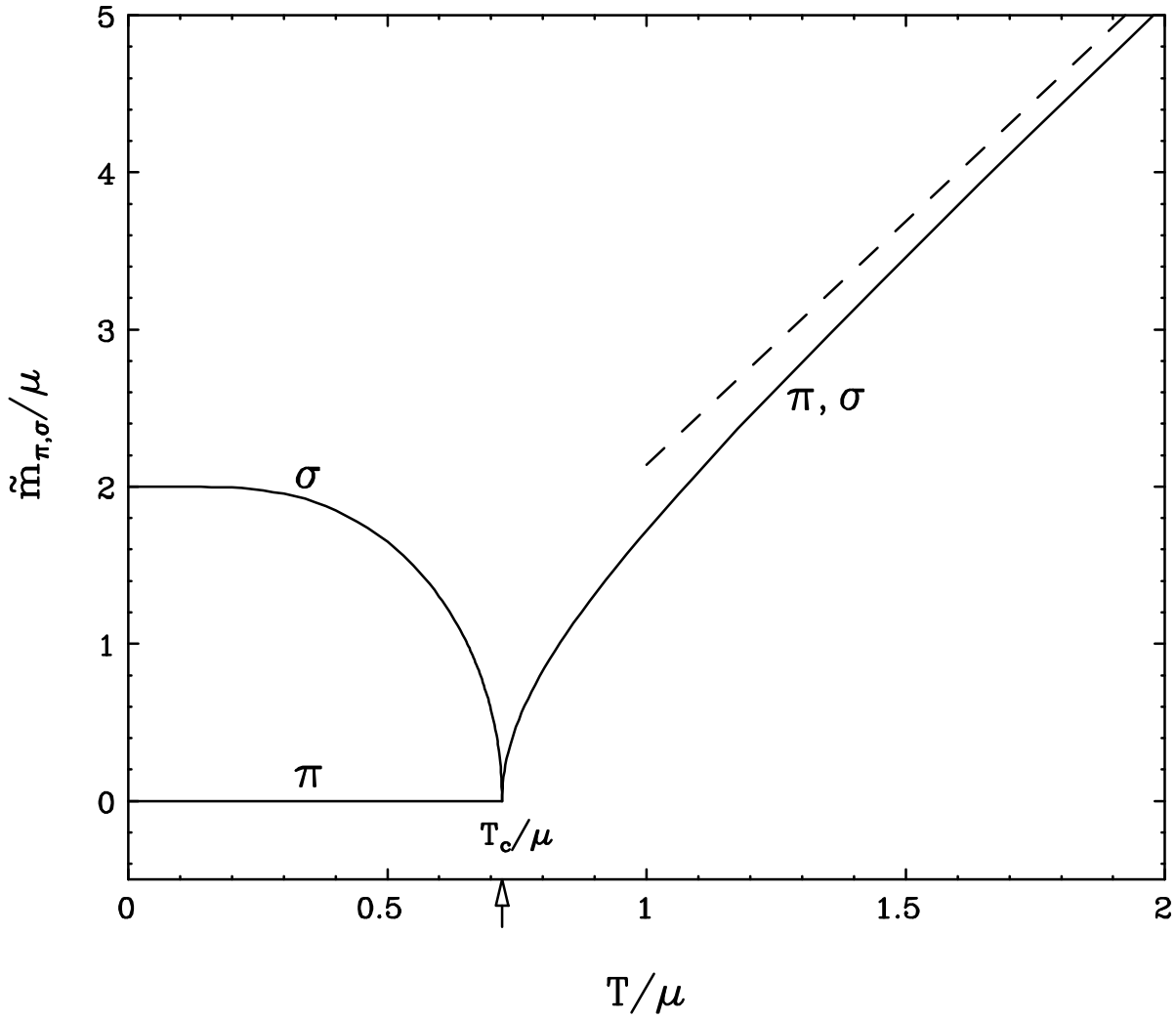


Figure 6

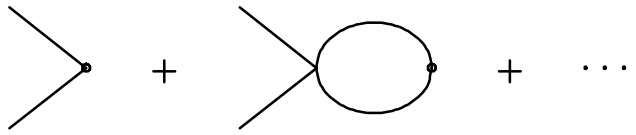

Figure 7